NKS-458
ISBN 978-87-7893-551-9

SOurce CHAracterizatiOn accounting for meTeorologIcal unCertainties (SOCHAOTIC) – first-year report

Jens Havskov Sørensen[1] (co-ordinator)
Henrik Feddersen[1]
Kasper Skjold Tølløse[1]
Rostislav Kouznetsov[2]
Mikhail Sofiev[2]
Andreas Uppstu[2]
Heiko Klein[3]
Magnus Ulimoen[3]
Lennart Robertson[4]
Jan Pehrsson[5]
Bent Lauritzen[6]
Dan Bohr[7]
Agnieszka Hac-Heimburg[7]
Carsten Israelson[7]
Einar Améen[8]
Anna Maria Blixt Buhr[9]
Jonas Lindgren[9]
Tuomas Peltonen[10]

[1]Danish Meteorological Institute (DMI)
[2]Finnish Meteorological Institute (FMI)
[3]Norwegian Meteorological Institute (MET Norway)
[4]Swedish Meteorological and Hydrological Institute (SMHI)
[5]PDC-ARGOS
[6]Technical University of Denmark (DTU)
[7]Danish Emergency Management Agency (DEMA)
[8]Norwegian Radiation and Nuclear Safety Authority (DSA)
[9]Swedish Radiation Safety Authority (SSM)
[10]Radiation and Nuclear Safety Authority (STUK)

April 2022

Abstract

In recent years, events have occurred in which radionuclides were detected by filter stations in European countries without knowledge on the origin of those radionuclides. In such cases, there is a need to locate potential release sites. However, if the release site is actually known, or if a potential release site has been localized by inverse methods, then there is an additional need to estimate the release rates from this location as a function of time for the various radionuclides detected.
While in the SLIM NKS project, methodologies were developed to localize an unknown source of radionuclides dispersed in the atmosphere, the SOCHAOTIC project develops methodologies, suited for operational use, by which characterization of the source, whose location is known, can be derived, i.e. to estimate the temporal release profiles of the radionuclides detected.
For operational use, nuclear decision-support systems should be extended with modules handling and analysing such monitoring data automatically, and conveying the data together with the geographical coordinates of the release point to the national meteorological centre accompanied by a request to estimate the temporal evolution of the release rates.
In the first year of SOCHAOTIC, the following results are obtained:

- Case studies identified and selected, viz. the ETEX-1 and the October 2017 case of Ru-106 in Europe. In addition, an artificial case is produced by running a dispersion model forward and calculating average concentrations at filter stations and gamma dose rates at nearby gamma stations.
- Methods for estimation of the temporal release profiles are developed, implemented and described.
- Deterministic numerical weather prediction model data are derived.
- Quality-controlled measurement data of ground-level concentration are obtained.
- The methods for source term characterization are applied by using the DERMA, MATCH, SILAM and SNAP atmospheric dispersion models.

Results are intercompared.

Key words

nuclear emergency preparedness, atmospheric dispersion modelling, source characterization, inverse modelling, concentration measurements, gamma dose measurements, uncertainty

NKS-458
ISBN 978-87-7893-551-9
Electronic report, April 2022

NKS Secretariat
P.O. Box 49
DK - 4000 Roskilde, Denmark
Phone +45 4677 4041
www.nks.org
e-mail nks@nks.org

SOurce CHAracterizatiOn accounting for meTeorologIcal unCertainties (SOCHAOTIC) – first-year report

First-year report of the NKS-B SOCHAOTIC activity

(Contract: AFT/B(20)3)

Jens Havskov Sørensen[1] (co-ordinator)
Henrik Feddersen[1]
Kasper Skjold Tølløse[1]

Rostislav Kouznetsov[2]
Mikhail Sofiev[2]
Andreas Uppstu[2]

Heiko Klein[3]
Magnus Ulimoen[3]

Lennart Robertson[4]

Jan Pehrsson[5]

Bent Lauritzen[6]

Dan Bohr[7]
Agnieszka Hac-Heimburg[7]
Carsten Israelson[7]

Einar Améen[8]

Anna Maria Blixt Buhr[9]
Jonas Lindgren[9]

Tuomas Peltonen[10]

[1]Danish Meteorological Institute (DMI)

[2]Finnish Meteorological Institute (FMI)

[3]Norwegian Meteorological Institute (MET Norway)

[4]Swedish Meteorological and Hydrological Institute (SMHI)

[5]PDC-ARGOS

[6]Technical University of Denmark (DTU)

[7]Danish Emergency Management Agency (DEMA)

[8]Norwegian Radiation and Nuclear Safety Authority (DSA)

[9]Swedish Radiation Safety Authority (SSM)

[10]Radiation and Nuclear Safety Authority (STUK)

Table of contents

Introduction

In recent years, several events have occurred in which radionuclides were detected by radiological filter stations in a number of European countries without any knowledge of the origin of those radionuclides. In such cases, there is a need to locate potential release sites by inverse dispersion modelling techniques. However, if the release site is actually known, or if a potential release site has been localized by inverse methods, then there is an additional need to estimate the release rates from this location as a function of time for the various radionuclides detected.

Two kinds of radiological monitoring networks exist, viz. filter and gamma stations. Filter stations detect radionuclide-specific time-average concentrations with high accuracy and low thresholds, however with long averaging periods (e.g. between one and seven days). Gamma stations produce time-average radiation doses in which the radionuclides are lumped together, and with lower accuracy and higher thresholds, however with short averaging periods (down to 10 minutes).

While in the SLIM NKS project, methodologies have been developed to localize an unknown source of radionuclides dispersed in the atmosphere and detected by a radiological monitoring network, the SOCHAOTIC project develops methodologies, suited for operational use, by which a characterization of the source, whose location is known, can be derived, i.e. to estimate the temporal release profiles of the radionuclides detected.

For operational use, nuclear decision-support systems should be extended with modules handling and analysing such monitoring data automatically, e.g. by employing the European Radiological Data Exchange Platform (EURDEP), and conveying the data together with the geographical coordinates of the release point to the national meteorological centre accompanied by a request to estimate the temporal evolution of the release rates.

In the first year of SOCHAOTIC, the following results are obtained:

- Case studies identified and selected, the ETEX-1 and the October 2017 case of Ru-106 in Europe. In addition, an artificial case is produced by running a dispersion model forward and calculating average concentrations at filter stations and gamma dose rates at nearby gamma stations.
- Methods for estimation of the temporal release profiles are developed, implemented and described.
- Deterministic numerical weather prediction (NWP) model data are derived from the European Centre for Medium-Range Weather Forecasts (ECMWF) as well as the non-hydrostatic high-resolution Harmonie model, corresponding to the selected cases.
- Quality-controlled measurement data of ground-level concentration are obtained.
- The methods for source term characterization are applied by using the DERMA, MATCH, SILAM and SNAP atmospheric dispersion models to the selected cases.
- Results are intercompared.

Atmospheric Dispersion Models

Danish Emergency Response Model of the Atmosphere (DERMA)

The Danish Emergency Response Model of the Atmosphere (DERMA) (Sørensen *et al.*, 2007; Sørensen, 1998) is a comprehensive numerical regional and meso-scale atmospheric dispersion model developed at the Danish Meteorological Institute (DMI). The model is used operationally for the Danish nuclear emergency preparedness, for which the Danish Emergency Management Agency (DEMA) is responsible (Hoe *et al.*, 2002). Besides, the model is employed for veterinary emergency preparedness (Sørensen *et al.*, 2000; 2001; Mikkelsen *et al.*, 2003; Gloster *et al.*, 2010a; 2010b), where it is used for assessment of airborne spread of animal diseases, e.g. foot-and-mouth disease. DERMA may also be used to simulate atmospheric dispersion of chemical substances, biological warfare agents and ashes from volcanic eruptions, and it has been employed for probabilistic nuclear risk assessment (Lauritzen *et al.*, 2006; 2007; Baklanov *et al.*, 2003; Mahura *et al.*, 2003; 2005).

The main objective of DERMA is to predict the dispersion of a radioactive plume and the accompanied deposition. However, the model may also be used in situations where increased levels of radioactivity have been measured but no information is revealed on a radioactive release. In such cases, inverse (adjoint) modelling may be applied whereby potential sources of radioactivity may be localised and release rates estimated.

The three-dimensional model is of Lagrangian type making use of a hybrid stochastic particle-puff diffusion description, and it is currently capable of describing plumes at downwind distances up to the global scale (Sørensen *et al.*, 1998). The model utilizes aerosol size dependent dry and wet deposition parameterisations as described by Baklanov and Sørensen (2001).

Currently, DERMA makes use of analysed and forecasted meteorological data of various deterministic versions at DMI of the NWP model Harmonie (Bengtsson *et al.*, 2017) covering North-western Europe, Greenland and the Faeroes, and from the global model developed and operated by the European Centre for Medium-range Weather Forecasts (ECMWF). Further, DERMA utilizes the COMEPS ensemble prediction system, which is based on the Harmonie model.

DERMA is interfaced with the Accident Reporting and Guidance Operational System (ARGOS) (Hoe *et al.*, 1999; 2002), a PC based nuclear decision-support system developed by the Prolog Development Center (PDC). The integration of DERMA with the ARGOS system is effectuated through automated online digital communication and exchange of data between the ARGOS system and the DMI High Performance Computing (HPC) facility.

Method Employed for Source Characterization

The temporal release profile of the various different radionuclides involved is estimated by using filter and gamma station measurement data and employing an atmospheric dispersion model.

Assume an overall start time t_0 and end time t_N of the release, and separate the release period $[t_0, t_N]$ in time bins (j), e.g. of one- or three-hour duration, and for each of these assume a unit release of each radionuclide (i) measured by the filter stations, see Figure 1.

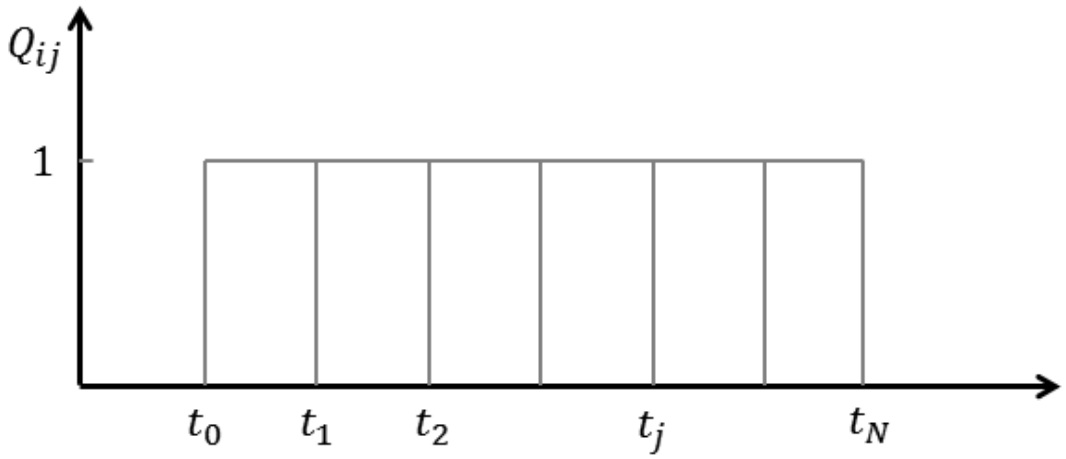

Figure 1 Time-binned unit release of radionuclide ***i***.

For each release time bin j, and for each radionuclide i, the atmospheric dispersion model is run forward in time calculating average activity concentrations c_{ijkl} at the filter stations k corresponding to their measurement periods l. Also, the average activity concentrations c_{ijkl} and deposition values d_{ijkl} are calculated at the gamma stations k corresponding to their measurement periods l. By using a semi-infinite gamma dose model, the contributions γ_{ijkl} to the gamma dose rates are calculated.

For each radionuclide i, a linear combination of the time-binned releases, with non-negative coefficients λ_{ij}, is assumed. For a given set of non-negative coefficients λ_{ij}, the predicted average concentration is calculated at filter stations,

$$C_{ikl} = \sum_j \lambda_{ij}\, c_{ijkl},$$

and predicted gamma dose rates at gamma stations,

$$\Gamma_{kl} = \sum_{ij} \lambda_{ij}\, \gamma_{ijkl}.$$

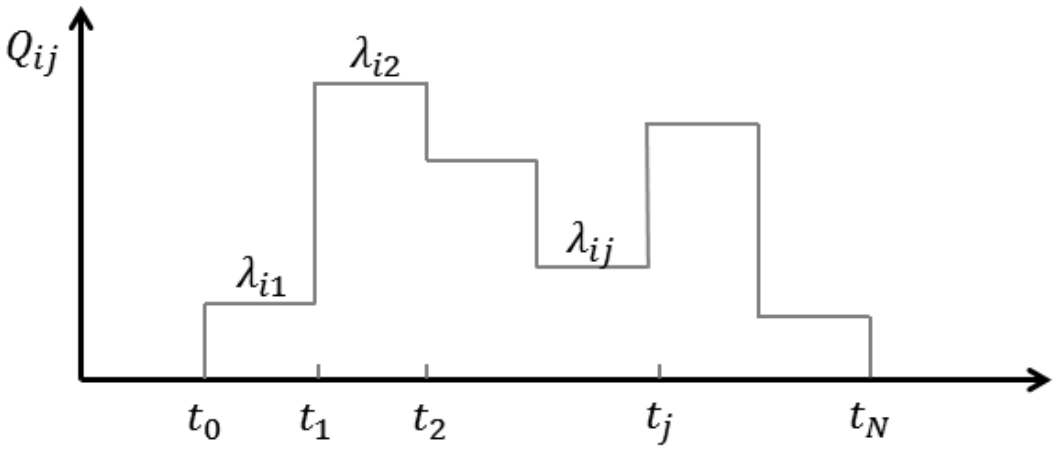

Figure 2 Estimated release rate of radionuclude ***i*** as function of time.

The corresponding piece-wise constant temporal profile of the source term is calculated for each radionuclide i, see Figure 2.

Uncertainty quantification

In both approaches described above, we need a quantitative estimate of σ_{ikl} to evaluate the likelihood. As described above, the uncertainty can be related to uncertainties due to both observation errors and modelling errors. The former may be known to some extent, but the unknown model uncertainties are typically dominating.

When the uncertainties are unknown, one option is to treat these as so-called *nuisance parameters*, which are unknown parameters that are not of direct interest. In that case, we need to consider the joint probability distribution $P\left(\boldsymbol{\lambda}, \boldsymbol{\sigma}_i \middle| \tilde{\mathbf{C}}_i, I\right)$ and then marginalize over the dimensions of $\boldsymbol{\sigma}_i$ to obtain the probability distribution for $\boldsymbol{\lambda}$. However, the problem is likely to be undetermined, if all elements of $\boldsymbol{\sigma}_i$ are treated as free parameters. Therefore, we instead examined three simple assumptions for $\boldsymbol{\sigma}_i$: (1) $\sigma_{ikl} = a$, (2) $\sigma_{ikl} = a\tilde{C}_{ikl}$, and (3) $\sigma_{ikl} = aC_{ikl}$. In all three cases, a is a constant, which is determined by the Monte Carlo algorithm. The two latter approaches are based on the idea that the model uncertainty should scale with the predicted concentration itself, while the idea behind the first approach is that the model might be better at predicting higher concentrations, and accordingly, one should give greater weights to these terms. We found that the first approach, i.e. assuming that the uncertainty is the same for all measurements, gives the best results.

Other considerations

The time bins included in the analysis are likely to cover a longer period than the actual release; otherwise, we would already know when the release took place. This means that the concentration fields from some of these bins may not coincide in time and space with the available measurements. If only a small fraction of the measurements is ”hit” by the plume, the corresponding coefficient is not properly constrained by the data, and therefore the Monte Carlo algorithm will tend to allow the release from these bins to vary unrestricted; i.e. only restricted by the prior distribution. In this study, we therefore only include the 50% of the time bins that affect most measurements; see a demonstration of this on the ETEX-1 case in the results section. This is a very simple approach and might not be generally applicable. As discussed in result section for the Loviisa case, we still see some time bins, where the parameters are not properly constrained, even after excluding the 50% of the time bins.

The result is also sensitive to the width of the time bins. It is not trivial to determine the ideal bin width a priori, since this will most likely depend on several different parameters: the number and duration of the measurements available, the distance travelled from release location to measurement stations, as well as the weather situation. For the ETEX case, we use $\Delta t = 3$ h, For the Loviisa case, we use $\Delta t = 3$ h, and for the Ru-106 case, we use $\Delta t = 6$ h.

We also include non-detections in our analysis by simply assuming that these are measurements of zero concentration. This is strictly not true, but if the detection limits are small compared to the numerical values of the non-zero detections, the assumption should be reasonable.

Bayesian approach

We use a Bayesian approach for estimating the source term, which has also been applied to source term characterization problems in previous studies (Le Brazidec *et al.*, 2020; Tølløse *et al.*, 2021). In contrast to these two studies, which aim at localizing the source, we assume that the location is known and instead aim at determining the temporal evolution in the source. The probability distribution for $\boldsymbol{\lambda}$ is obtained by Bayes' theorem

$$P\left(\boldsymbol{\lambda}\middle|\tilde{\mathbf{C}},\tilde{\boldsymbol{\Gamma}},I\right)=\frac{P(\boldsymbol{\lambda}|I)\,P\left(\tilde{\mathbf{C}},\tilde{\boldsymbol{\Gamma}}\middle|\boldsymbol{\lambda},I\right)}{P\left(\tilde{\mathbf{C}},\tilde{\boldsymbol{\Gamma}}\middle|I\right)}\propto P(\boldsymbol{\lambda}|I)\,P\left(\tilde{\mathbf{C}},\tilde{\boldsymbol{\Gamma}}\middle|\boldsymbol{\lambda},I\right),$$

where I is any available background information about the release, and $\tilde{\mathbf{C}}$ and $\tilde{\boldsymbol{\Gamma}}$ are the measured concentrations and gamma doses, respectively. $P\left(\boldsymbol{\lambda}\middle|\tilde{\mathbf{C}},\tilde{\boldsymbol{\Gamma}},I\right)$ is the *posterior* probability distribution for the coefficients $\boldsymbol{\lambda}$, $P(\boldsymbol{\lambda}|I)$ is the *prior* probability distribution for the coefficients, and $P\left(\tilde{\mathbf{C}},\tilde{\boldsymbol{\Gamma}}\middle|\boldsymbol{\lambda},I\right)$ is the likelihood (the probability of observing $\tilde{\mathbf{C}},\tilde{\boldsymbol{\Gamma}}$ given a proposed set of coefficients, $\boldsymbol{\lambda}$). Finally, $P\left(\tilde{\mathbf{C}},\tilde{\boldsymbol{\Gamma}}\middle|I\right)$ is called the evidence. The evidence is independent of $\boldsymbol{\lambda}$ and, for our purpose, it is merely an unknown normalization constant.

For a high-dimensional $\boldsymbol{\lambda}$, it is not computationally feasible to systematically explore all parts of the parameter space. Instead, the posterior probability distribution can be sampled using Markov Chain Monte Carlo methods (MCMC) such as Metropolis-Hasting or Gibbs (Hastings, 1970; Casella and George, 1992). The basic idea behind these methods is to iteratively propose source term models and *accept* them with a probability proportional to $P\left(\boldsymbol{\lambda}\middle|\tilde{\mathbf{C}},\tilde{\boldsymbol{\Gamma}},I\right)$. This way, areas with high probability are more likely to be explored, and therefore $P\left(\boldsymbol{\lambda}\middle|\tilde{\mathbf{C}},\tilde{\boldsymbol{\Gamma}},I\right)$ can be estimated even for a high-dimensional $\boldsymbol{\lambda}$. When a sufficient number of models are accepted, the posterior statistics can be extracted from the selection of accepted models. In this study, we use the Hamiltonian Monte Carlo (HMC) method No U-Turn Sampling (NUTS), (Hoffman and Gelman, 2014), which is implemented in the python library PyMC3 (Salvatier *et al.*, 2016). HMC methods generally have an advantage over random-walk based MCMC methods, because the model proposals are not generated by a random walk but instead based on an estimate of a functional form of $P\left(\boldsymbol{\lambda}\middle|\tilde{\mathbf{C}},\tilde{\boldsymbol{\Gamma}},I\right)$. In order to sample the probability distribution, we need to assume functional forms for the prior distribution, $P(\boldsymbol{\lambda}|I)$ and the likelihood, $P\left(\tilde{\mathbf{C}},\tilde{\boldsymbol{\Gamma}}\middle|\boldsymbol{\lambda},I\right)$.

Prior probability distribution

We assume that very little information about the release is available a priori. Thus, determining a prior distribution for the coefficients λ_{ij} is not trivial. However, we assume the following: (1) all λ_{ij} are non-negative, and (2) an a priori estimate of λ_{ij} might be very uncertain, and for some ij, the true λ_{ij} is likely to be zero; therefore, $P(\boldsymbol{\lambda}|I)$ should allow for variation over several orders of magnitude.

We assume a log-normal distribution, corresponding to assuming a Gaussian distribution for the variable $X_{ij}=\log(\lambda_{ij})$. This will ensure positive values and allow for variation over orders of magnitude, given that a sufficiently large standard deviation is chosen.

The mean of the normal distribution of X_{ij} is estimated by providing a first guess of the magnitude of the release, S_0, i.e. the total amount released of a radionuclide, and an estimated duration of the release, T. These estimates are then used to define a first guess of a

characteristic release rate, $Q_0 = S_0/T$. Since each bin has been run with unit releases, the unit-less coefficient λ_{ij} has the same numerical value as the release rate, and therefore we have $\mu_X = \log(Q_0/(1\ \text{Bq s}^{-1}))$. The standard deviation is then chosen based on the consideration that at least a few orders of magnitude should be included in $\mu_X \pm \sigma_X$. We choose to include two orders of magnitude on each side of μ_X, i.e. $\sigma_X = 2\log(10)$, where the factor $\log(10)$ merely compensates for the fact that the natural logarithm is used.

For ETEX1, we use $S_0 = 10^{14}$ ng, for the Ru-106 case, we use $S_0 = 10^{14}$ Bq, and for the Loviisa, we use $S_0 = 10^{17}$ Bq. In this study, these first guesses are based on the actual releases or, in the Ru-106 case, on estimates from other studies. In a real case application, one would make this estimate based on knowledge about the type of nuclear power plant and type of accident. However, the method is not very sensitive to this estimate as long as σ_X is sufficiently large.

Likelihood

We first consider a Gaussian likelihood

$$P(\tilde{\mathbf{C}}, \tilde{\mathbf{\Gamma}}|\boldsymbol{\lambda}, I) = \left(\prod_{ikl} \frac{1}{\sqrt{2\pi}\sigma_{ikl}}\right) e^{-\frac{1}{2}\sum_{ikl}\left(\frac{\tilde{C}_{ikl}-C_{ikl}}{\sigma_{ikl}}\right)^2} \left(\prod_{kl} \frac{1}{\sqrt{2\pi}\sigma_{kl}}\right) e^{-\frac{1}{2}\sum_{kl}\left(\frac{\tilde{\Gamma}_{kl}-\Gamma_{kl}}{\sigma_{kl}}\right)^2},$$

where σ_{ikl} and σ_{kl} are the uncertainties of filter and gamma data, respectively. The uncertainties are due to both measurement errors and modelling errors, and can be written as $(\sigma_{ikl})^2 = (\sigma_{ikl}^{\mathrm{m}})^2 + (\sigma_{ikl}^{\mathrm{o}})^2$, where the superscripts m and o denote modelling and observation uncertainties, respectively.

Second, we consider a log-normal likelihood, which has been argued to be more suited for atmospheric dispersion problems due to the variation over several orders of magnitude (Liu *et al.*, 2017; Le Brazidec *et al.*, 2020). This essentially corresponds to assuming a Gaussian distribution for the logarithm of the concentrations and gamma doses, respectively

$$P(\log(\tilde{\mathbf{C}}), \log(\tilde{\mathbf{\Gamma}})|\boldsymbol{\lambda}, I) = \left(\prod_{ikl} \frac{1}{\sqrt{2\pi}\sigma_{ikl}}\right) e^{-\frac{1}{2}\sum_{ikl}\left(\frac{\log\left(\frac{\tilde{C}_{ikl}}{C_{ikl}}\right)}{\sigma_{ikl}}\right)^2} \left(\prod_{kl} \frac{1}{\sqrt{2\pi}\sigma_{kl}}\right) e^{-\frac{1}{2}\sum_{kl}\left(\frac{\log\left(\frac{\tilde{\Gamma}_{kl}}{\Gamma_{kl}}\right)}{\sigma_{kl}}\right)^2}.$$

Here, σ_{ikl} and σ_{kl} are the uncertainties of the logarithm of the filter and gamma data, respectively. Thus, these should not be mistaken with the uncertainties in the Gaussian likelihood above.

In this first part of the project, we have ignored gamma dose measurements, and therefore the release of each different particle can be treated as a separate problem. Further, in practice, a correction to the log-normal distribution is necessary, because both measurements and model predictions can be zero. Therefore, we follow one of the suggested approaches by Liu *et al.* (2017) where a small non-zero number is added to the concentration values. The resulting expressions are

$$P(\tilde{\mathbf{C}}_i|\boldsymbol{\lambda}_i, I) = \left(\prod_{kl} \frac{1}{\sqrt{2\pi}\sigma_{ikl}}\right) e^{-\frac{1}{2}\sum_{kl}\left(\frac{\tilde{C}_{ikl}-C_{ikl}}{\sigma_{ikl}}\right)^2}, \text{(Gaussian)}$$

$$P(\log(\tilde{\mathbf{C}}_i)|\boldsymbol{\lambda}_i, I) = \left(\prod_{kl} \frac{1}{\sqrt{2\pi}\sigma_{ikl}}\right) e^{-\frac{1}{2}\sum_{kl}\left(\frac{\log\left(\frac{\tilde{C}_{ikl}+\varepsilon_i}{C_{ikl}+\varepsilon_i}\right)}{\sigma_{ikl}}\right)^2}, \text{(log-normal)}$$

where $\tilde{\mathbf{C}}_i$ is the matrix containing the measurements of the *i*'th radionuclide, and $\boldsymbol{\lambda}_i$ is the vector containing the coefficients for the same radionuclide; ε_i is a small number, e.g. the detection limit of the filter station. For the ETEX-1 case, we use the detection limit $\varepsilon_i = 0.01$ ng/m^3, and for both the Ru-106 and Loviisa cases, we use $\varepsilon_i = 0.1$ mBq/m^3, which is the order of magnitude of the average detection limit in the Ru-106 dataset.

Multi-scale Atmospheric Transport and Chemistry model (MATCH)

The Multi-scale Atmospheric Transport and Chemistry model (MATCH) (Robertson *et al.*, 1999) is multi-purpose Eulerian chemical transport model (CTM) developed by the SMHI. The model is used for emergency application such as nuclear and natural events (volcanos), aerosol dynamics and optics (Andersson *et al.*, 2015), complex chemistry, and data assimilation (Robertson and Langner, 1998; Kahnert, 2008; Kahnert, 2018). The MATCH model is used operationally for chemical forecasts in CAMS (Copernicus Atmospheric Monitoring Service) and for SSM (Swedish Radiation Safety Authority) serving the ARGOS system needs (Hoe *et al.*, 1999; 2002). Other applications are studies for air quality and health issues in climate projections. In most applications MATCH is used as a limited-area model on various possible scales, but also for global applications.

The MATCH model is basically an Eulerian model but for emergency applications a Lagrangian particle model is used in the near field of the emission location.

A wide range of possible driving meteorological data is applicable like analyses and forecasts from HARMONIE, IFS (ECMWF) and WRF.

Method Employed for Source Characterization

In these applications we have applied so called Poor-man source inversion. This is a simplification of the complete 4Dvar where only one iteration is made followed of bias correction. In principle we run the adjoint model forced by the measurements where also adjoint gamma-dose may come in. We then pick up the adjoint solution for the column associated with the defined source location. A time series of such columns are then retrieved. The concept applies well for a Eulerian model. We now assume that these columns represent the source profile with an unknown scale factor to be determined. This is derived by running the forward model given the source suggestion from the adjoint run. When comparing the model and measurements we assume that there is only a scale factor other than implicitly one that is missing in a quadratic error sense.

Bringing this into a mathematical language we may first consider the transport model in a general form,

$$x_{t+1} = M_t x_t + P q_t$$

where x_t is the model state, M_t is the transport equations and P an injector matrix to place the source column q_t at the right location in the model grid. We now assume a cost function of the following form,

$$J(x_t) = \sum_t^T \frac{1}{2}(q_t - q_{bt})^T B^{-1}(q_t - q_{bt}) + \frac{1}{2}(Hx_t - y_t)^T O^{-1}(Hx_t - y_t)$$

that represents quadratic penalties for deviation from an initial source column guess and a penalty for deviation from the observations. Here the observation operator H is important, that maps the model grid values to the observation locations and in addition, when valid, perform gamma dose transform of the model nuclide specific model state. If we then bring the model as above a strong constraint we mat write,

$$J(x_t) = \sum_t^T \frac{1}{2}(q_t - q_{bt})^T B^{-1}(q_t - q_{bt}) + \frac{1}{2}(Hx_t - y_t)^T O^{-1}(Hx_t - y_t) + \lambda_{t+1}^T(Mx_t + Pq_t - x_{t+1})$$

Here λ represents the co-state or the adjoint state. The cost function will have minimum where the gradient with respect to the model state, x_t, is zero that lead us to the adjoint transport model,

$$\lambda_t = M_t^T \lambda_{t+1} + H^T O^{-1}(Hx_t - y_t)$$

It is worth to make short stop here and conclude that the adjoint state is integrated backward in time driven by the adjoint model equations (M_t^T) and forced by the deviation between model and measurements, transferred through the transpose (adjoint) of the observation operator, that in turn may include adjoint gamma dose rates.

We could from above also derive the gradient with respect to a specific source column q_t,

$$\nabla J_{q_t} = P^T \lambda_t + B^{-1}(q_t - q_{bt})$$

that is derived from the adjoint state, where P^T turns in to an extractor of a column that belongs to the source location. For a full variational assimilation the second term on the right side will be important, while in the Poor-man case this will disappear. We may stepwise update the source columns,

$$q_t^{n+1} = q_t^n - \alpha \nabla J_q$$

where α is a scaling factor. The source columns may then be incrementally updated by forward and adjoint runs. The Poor-man approach does then simplify by just making one iteration,

$$
\begin{aligned}
q_t^0 &\equiv q_{bt} = 0 \\
q_t^{n+1} &= -\alpha \nabla J_q = -\alpha \lambda_t \\
\alpha &= ?
\end{aligned}
$$

where α initially assumed to be unit. One forward run then will determine how good this assumption appeared to be. Then setting up quadratic cost function with the unknown factor α,

$$
J(\alpha) = \sum_t^T (\alpha H x_t - y_t)^T (\alpha H x_t - y_t)
$$

and just using Newton-Raphson algorithm we could iteratively determine best α,

$$
\begin{aligned}
\alpha^{n+1} &= \alpha^n - \nabla J(\alpha) / J^{''}(\alpha) \\
\alpha^{n+1} &= \alpha^n - \sum_t^T H x_t^T (\alpha H x_t - y_t) / \sum_t^T (H x_t)^T H x_t
\end{aligned}
$$

This procedure may be iterated a couple of turns with a forward model run in between.

One element to consider is that the source term derived above is not directly the source intensity but the concentration that the source intensity would lead to. Converting from concentrations to source intensities could then in the final output be a bit arbitrary.

The gamma dose operator is derived from Heinonen (2017) and references therein with tabulated gamma energies and range parameters. A generic gamma dose stencil is for each nuclide and model layer derived integrating in a surrounding of the cell coordinate then assumed applicable to any grid cell coordinate. The adjoint is the transpose of this generic gamma dose operator.

System for Integrated modeLling of Atmospheric coMposition (SILAM)

SILAM (System for Integrated modeLling of Atmospheric coMposition, , last access: 5 Jan 2021) is an offline 3D chemical transport model (Sofiev *et al.*, 2015). SILAM features a mass-conservative positive-definite advection scheme that makes the model suitable for long-term runs. The model can be run at a range of resolutions starting from a kilometre scale in a limited-area up to a global coverage. The vertical structure of the modelling domain consists of stacked layers starting from the surface. The layers can be defined either in z- or hybrid sigma-pressure coordinates. The model can be driven with a variety of NWP (numerical weather prediction) or climate models.

The model is used for emergency-response applications and includes radioactive transformation mechanism and various passive tracers.

Method Employed for Source Characterization

The source characterization is performed through optimization of the time-slot specific model emission. The cost function of the optimization is the sum of the squared model errors, to which an additional regularization term can be added. Here, the regularization term is set to be proportional the sum of the squares of the differences between the emission coefficients of consecutive time slots. A suitable trade-off between the smoothness of the optimized temporal evolution of the emission and the model to measurement error is found through an L-curve method, which utilizes a plot of the model error versus the residual error. The method can be used to effectively remove the length of the emission time slot from the degrees of freedom of source characterization. In other words, a short time slot of one hour can be applied, with the regularization helping to avoid overfitting in terms of temporal complexity.

The optimization procedure itself is based on a standard application of the L-BFGS-B algorithm, as applied within the Python package scipy. As the method is computationally light, at least for the cases studied here, a brute force method of iterative application of random initial guesses spanning up to ten orders of magnitude is applied to ensure that good optimization results are achieved. Although the vertical emission profile is fixed, the impacts profile alterations can be studied through separate simulation runs.

Severe Nuclear Accident Program (SNAP)

The Norwegian Meteorological Institute (MET-Norway) is responsible for modelling atmospheric dispersion of radioactive debris in the event of a nuclear emergency related to a nuclear accident or detonation. An additional task of the MET-Norway in a nuclear emergency is to identify unknown sources of radiation indicated by elevated levels of measurement. The basic tool used by the MET-Norway for such events is the Severe Nuclear Accident Program (SNAP) (Bartnicki *et al.*, 2011; Klein and Bartnicki, 2018).

The SNAP model was developed at the MET-Norway in 1994 as a Lagrangian particle model. The present version is fully operational at the MET-Norway and takes into account atmospheric transport and deposition of gases, noble gases and particles of different size and density emitted during nuclear accidents or explosions. SNAP can also be run remotely by experts from the Norwegian Radiation and Nuclear Safety Authority (DSA) where the Norwegian Crisis Committee is located.

Once released into the air, radioactive gases and particles are subject to advection, turbulent diffusion and deposition (dry and wet). In the SNAP calculations, the advection process is immediately followed by the diffusion process. A random walk approach is used to parameterise horizontal and vertical diffusion. When large and dense particles are released, gravitational settling is more effective than vertical diffusion, and this process is taken into account. The SNAP model has been used both for simulations of historical events, e.g. nuclear detonations in Novaya Zemlya, Chernobyl Accident (Bartnicki *et al.*, 2016), and real-time simulations, e.g. the Fukushima accident. It was tested in the ETEX-1 experiment and showed good agreement with observations (Saltbones *et al.*, 1998). SNAP is the dispersion model currently used by the MET-Norway in the Center of Excellence: CERAD CoE.

Method Employed for Source Characterization

The temporal release characteristics of the release is estimated by using the observations from air filter stations and gamma stations. The release is assumed consisting of releases at disjoint time bins t_j in $[t_0, t_n]$ where each bin has a duration of one hour. These time bins are

illustrated by Figure 1. The SNAP model is run forwards assuming a constant unit release of the radionuclides for each time bin t_j from a predetermined location, such as a suggested facility following the methods developed during the SLIM project. Each model run is then co-located with observations to form the source-receptor matrix M_{ij}.

$$M_{ij} = q_j(o_i)$$

where q_j is the result of the unit release at each location and o_i is the location of the observation. The release characteristics is described by the linear system

$$b_i = \sum_j M_{ij}\, x_j$$

where b_i describes the observations and x_j is the coefficients for each unit release. This is the approach given by Seibert (2001) with a zero a-priori and without the additional normalisation constraints based on smoothness of the source term.

The linear system of the above equation may be ill-posed and is solved using a non-negative least squares solver such that the solution

$$\min\left(\left|\left|M\,x - b\right|\right|_2\right)$$

$$x \geq 0$$

is the best approximation to the temporal release characteristics.

For handling gamma observations, the linear system may be augmented by setting elements of M_{ij} as gamma contributions from the species from each time bin t_j and let elements of b_i contain the gamma observations. This creates a linear dependence between the released species which may constrain the solutions. Gamma dose contributions can be calculated from the 10 lowest levels of the activity concentration (capturing >99% of the dose contribution from air) and the deposition.

Penalization and balancing

The solver may not behave optimally when there are large amounts of non-detections compared to detections at the stations. To balance and ensure the release does not optimise for no released activity, a penalty can be applied to some observations by multiplying both the row in M and the entry in b with a penalty:

$$M[i,:] := \sigma_i\, M[i,:]$$

$$b[i] := \sigma_i\, b[i]$$

where $\sigma_i \in [0,1]$ is the penalty parameter which can be used for assigning lower weights to non-detections in preference to detections well above the detection limit. The σ parametrisation may also be used for balancing the order of magnitude between gamma and air filter observations in the case these two are combined.

Semi-infinite Gamma Dose Model

The gamma ray flux at point **r** originating from the in-air or deposited concentration of a nuclide emitting radiation at energy E is calculated from the expression (CERC, 2012)

$$\Phi(\mathbf{r}, E) = \int \frac{f(E)\ c(\mathbf{r}')\ B(E, \mu(E)|\mathbf{r} - \mathbf{r}'|)\ \exp(-\mu(E)|\mathbf{r} - \mathbf{r}'|)}{4\pi|\mathbf{r} - \mathbf{r}'|^2} d\mathbf{r}', \quad (1)$$

where $c(\mathrm{r}_0)$ is the concentration of the nuclide, $f(E)$ is the branching ratio, $B(E, \mu(E)|\mathbf{r} - \mathbf{r}_0|)$ is the build-up factor, and $\mu(E)$ is the linear attenuation coefficient. In the dose rate calculator, the build-up factor is based on Berger's expression, i.e.

$$B(E, \mu(E)|\mathbf{r} - \mathbf{r}'|) = 1 + a(E)\mu|\mathbf{r} - \mathbf{r}'| \exp(b(E)\mu(E)|\mathbf{r} - \mathbf{r}'|), \quad (2)$$

where $a(E)$ and $b(E)$ are fitting constants that are readily available as tabulated data (CERC, 2012). In the atmosphere, $\mu(E)$ is not a constant, but varies as a function of air density, which in turn mostly depends on the height above sea level. $\mu(E)$ is calculated from the mass attenuation coefficient $\mu_0(E)$ through $\mu(E) = \mu_0(E)\rho_{\mathrm{air}}$, where ρ_{air} is the average air density between the source and point **r**. In the dose rate model, the air density is simply taken from a standard atmosphere.

Berger's expression and the corresponding fitting constants are strictly speaking not valid when the attenuation coefficient depends on **r**, but as the air density is varying only slowly as function of altitude compared to the scale of attenuation of gamma radiation in the atmosphere, the resulting error is expected to be small. The benefit of the method is that the dose rate calculator can be applied for any height above surface, even for typical flight altitudes, where the attenuation coefficient is only a fraction of the value at the surface.

The effective dose rate D at energy E is calculated from $\Phi(\mathbf{r}, E)$ based on

$$D(\mathbf{r}, E) = C(E)\ \mu_{\mathrm{abs}}(E)\ E\ \Phi(\mathbf{r}, E), \quad (3)$$

where μ_{abs} is an energy-dependent absorption coefficient and $C(E)$ a conversion factor from dose rate to effective dose rate.

The dose rate calculator approximates the radioactive cloud to be semi-infinite in the horizontal plane, which is a reasonable approximation for standard dispersion model output, as the horizontal size of the computational cell of a dispersion model is typically much larger than the relevant length scale of the attenuation. In the dose rate calculator, to simplify the calculations and to increase the computational speed, the height above the surface is approximated to equal the height above the sea level, which is a reasonable approximation for most parts of the world. If the dispersion model output is given in terms of hybrid levels, the levels are converted to height using the air density of a standard atmosphere. These approximations allow for performing the integration of Eq. 1 through pre-computed integration weights $w_{\mathrm{dr},i}(E)$, i.e.

$$\Phi(h_{dr}, E) = f(E) \sum_i w_{\mathrm{dr},i}(E)\ c_i, \quad (4)$$

where h_{dr} is the requested height for the dose rate calculation, i is the layer index of the dispersion model output, and c_i is the concentration of the nuclide inside layer i. The weights w_i are calculated using cylindrical coordinates (h, ρ, φ) from

$$w_{\mathrm{dr},i}(E) = \int_{h_{i,1}}^{h_{i,2}} \int_{0}^{\rho_{max}} \frac{\rho \; B(E, \mu(E) r(h,\rho)) \;\; \exp(-\mu(E) r(h,\rho))}{2 r(h,\rho)^2} d\rho \; dh, \quad (5)$$

where $\rho_{max} \rightarrow \infty$, and we have defined $r \equiv ((h - h_{dr})^2 + \rho^2)^{\frac{1}{2}}$. $h_{i,1}$ and $h_{i,2}$ are the lower and upper bounds of layer i, respectively. In the expression, the dependency on the polar angle φ has already been integrated out. However, the lack of an analytical solution prevents from doing that for the radial distance ρ.

Currently, instead, the radial part of the integral is computed numerically, with ρ_{max} set to 1500 m. While performing the numerical integration, the lengths of the integration steps in the h and ρ directions are optimized based on the magnitude of μ. The integration weights are calculated separately for in-air and deposited concentrations of nuclides.

Because of the approximation of taking the air density from a standard atmosphere, Eq. 5 needs to be solved only at the start of the dose rate calculation, but independently for all output heights h_{dr} and gamma emission energies E. However, tabulated values for $\mu_0(E)$, $a(E)$ and $b(E)$ exist only for specific energies, and in its two-dimensional form, the integral is also somewhat heavy computationally. Thus it is beneficial to perform the calculation of the vertical integration weights for a restricted number of different energies, with interpolation of the weights applied for all intermediate emission energies. The weights $w_{dr,i}$ are computed for all the energies listed in Table 1, rather than for all of the emission energies of all of nuclides in the output of the dispersion model. Each emission at energy E_{ems} is set to contribute to the total emission through a linear combination of the closest pre-computed values, i.e. weights for different pre-computed energies can be 3 defined as

$$w_{\text{ems-}} = \frac{\exp(E_{\mathrm{ems}}) - \exp(E_{-})}{\exp(E_{+}) - \exp(E_{-})} \; f(E_{\mathrm{ems}}) \quad (6)$$

$$w_{\mathrm{ems+}} = (1 - w_{\text{ems-}}) \; f(E_{\mathrm{ems}}), \quad (7)$$

if the growth of the gamma flux rate as function of energy is approximated to be exponential. E_{-} is the closest pre-computed energy value below the emission energy E_{ems} and E_{+} is the closest pre-computed energy value above it. w_{ems-} and w_{ems+} are the corresponding weights assigned for the precomputed energies. Final energy-dependent weights w_{ems} are acquired by summing the individual weights obtained for all the gamma emission energies of a specific nuclide. By combining Eqs. 4, 6, and 7 we end up with the expression for the total gamma ray dose rate $D_n(h_{dr})$ originating from the concentration of nuclide n, i.e.

$$D_n(h_{\mathrm{dr}}) = \sum_{i,j} C(E_j) \; \mu_{\mathrm{abs}}(E_j) \; E_j \; w_{\mathrm{ems},j} \; w_{\mathrm{dr},i}(E_j) \; c_i, \quad (8)$$

where the index j runs over all the energies in Table 1 and i over all the vertical layers of the dispersion model output. As discussed, the weights $w_{ems,j}$ and $w_{dr,i}(E_j)$ need to be calculated only at the start of the run. The emission energies E_{ems} and the corresponding branching ratios $f(E_{ems})$ are obtained from a database maintained by STUK.

Table 1. Tabulated values of the parameters of the dose rate calculation (CERC, 2012). μ_{0m} is the linear attenuation coefficient at sea level.

E (MeV)	μ_{0m} (1/m)	a	b	μ_{abs} (Gy m^2)	C (Sv/Gy)
0.01	0.623	0.025	-0.0464	7.43×10^{-16}	0.00296
0.015	0.187	0.0947	-0.0484	3.12×10^{-16}	0.0183
0.02	0.0893	0.2652	-0.0463	1.68×10^{-16}	0.0543
0.03	0.0411	1.055	-0.0192	0.721×10^{-16}	0.191
0.05	0.0253	3.498	0.0729	0.323×10^{-16}	0.557
0.065	0.0226	4.209	0.1169	0.278×10^{-16}	0.63
0.1	0.0195	4.033	0.1653	0.371×10^{-16}	0.765
0.2	0.0159	2.678	0.1678	0.856×10^{-16}	0.703
0.5	0.0112	1.748	0.1014	2.38×10^{-16}	0.689
1.0	0.00821	1.269	0.0559	4.47×10^{-16}	0.732
1.5	0.00668	1.040	0.0338	6.12×10^{-16}	0.765
2.0	0.00574	0.891	0.0215	7.50×10^{-16}	0.791
4.0	0.00398	0.5879	0.0022	12.0×10^{-16}	0.850
10	2.65e-3	0.3113	-0.0194	23.1×10^{-16}	0.935

ETEX-1

After the Chernobyl accident in April 1986 and the adoption of the Convention on Early Notification of a Nuclear Accident (IAEA, 1986), the International Nuclear Safety Advisory Group (INSAG) of the International Atomic Energy Agency (IAEA) recommended inter alia that the IAEA should, in collaboration with the World Meteorological Organisation (WMO), review and intercalibrate the models of atmospheric transport of radionuclides over short and long distances and of radionuclide deposition on terrestrial surfaces, and establish a database for validation studies of these models.

Following this recommendation, the joint IAEA/WMO Atmospheric Transport Model Evaluation Study (ATMES) was initiated in November 1986. The objective of ATMES was to compare the evolution of the radioactive cloud (I-131 and Cs-137) with the evolution predicted by mathematical models for atmospheric dispersion, using as input only the estimated source term of the Chernobyl accident.

The ATMES suffered, however, from a number of weaknesses regarding lack of monitoring data and large uncertainties regarding the source term. Therefore, it was decided to carry out a tracer experiment in Europe. The sponsoring organisations were the European Commission (EC), the World Meteorological Organization (WMO) and the International Atomic Energy Agency (IAEA), and later joined by the US Department of Energy (USDOE).

The experiment was named ETEX, European Tracer Experiment (Graziani *et al.*, 1998; ETEX web-site, 2019). It was designed to test the readiness of interested services to respond in the case of an emergency, to organise the tracer release and compile a data set of measured air concentrations and to investigate the performance of long-range atmospheric transport and dispersion models using that data set. In total, thirty-six organisations around the world were involved in the project.

Sampling network

The sampling network consisted of 168 ground-level sampling stations in western and eastern Europe. National meteorological services hosted the samplers at a number of WMO synoptic stations over their territory. Thus, ETEX could take advantage of this existing network, which is homogeneously distributed throughout Europe and linked to the WMO.

A final number of 168 sampling stations were selected, almost all located at existing WMO stations. Three samplers were located in the North Sea: one on a Dutch oil platform, the other two on gas platforms. The average spacing between two sampling stations in the resulting configuration was about 80 km.

Each station was labelled with one or two letters identifying the Country where it was located, and numbered sequentially.

It was planned to start the sampling operations at each station about 6 hours before the expected time of tracer arrival to obtain contemporaneous measurements of the tracer background levels and to ensure that the plume arrival was not missed. Each station was designed to sample over a period of 72 consecutive hours (24 three-hour samples), with sampling starting time progressively delayed from West to East. The stations closest to the source started sampling 3 hours before the release start; the most distant stations ended sampling 90 hours after the release start. The sampling network is depicted in Figure 3.

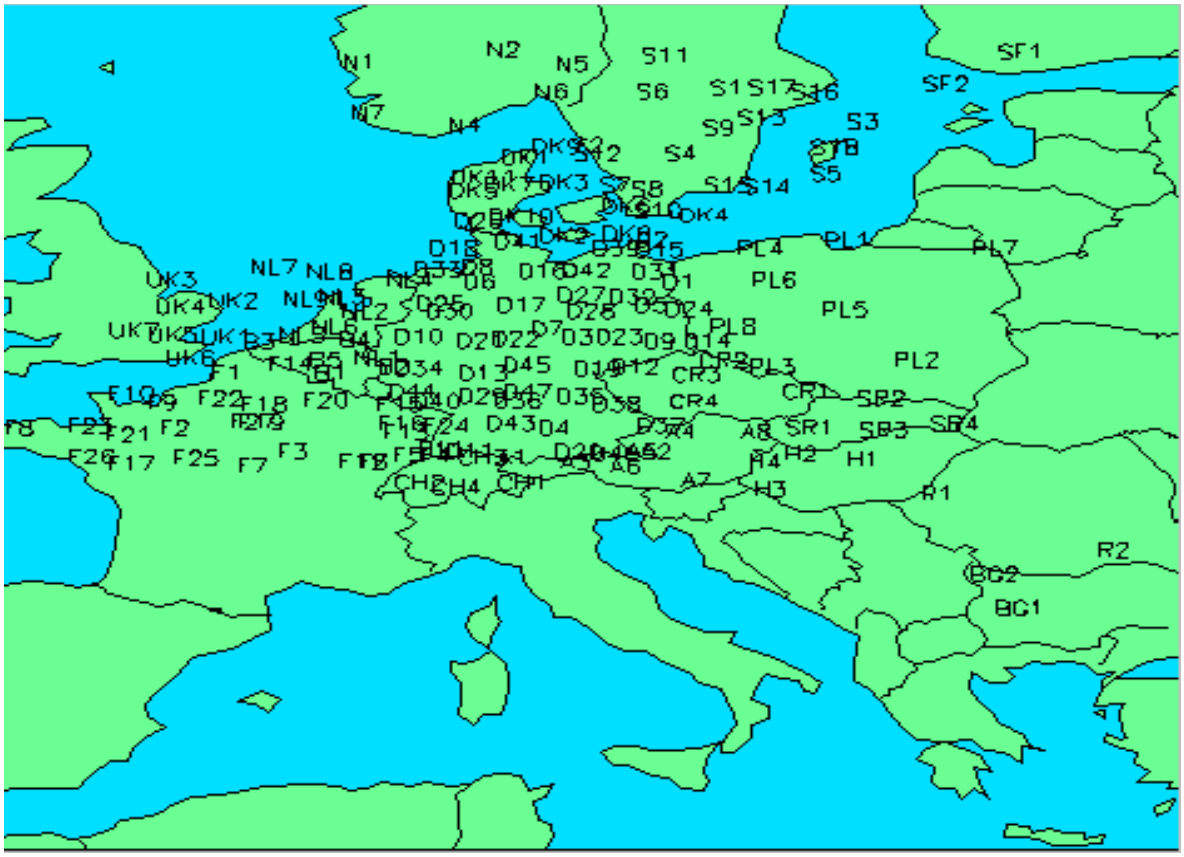

Figure 3 ETEX Sampling network (ETEX web-site, 2019).

Synoptic situation

Weather predictions suggested the following conditions on Sunday 23 October, 1994:

- the presence of a rather strong West to South-westerly flow, advecting the tracer during the experiment over several tracer stations
- no centre of high- or low-pressure, and no extending ridges or troughs, would have passed close to the release site
- no frontal systems would have passed the release site shortly before, during or after the release

Therefore, on Friday 21 October, 1994, the alert procedure was started.

23 October, 1994

A deep low, 975 hPa, to the East of Scotland was slowly moving north, maintaining a strong south-westerly flow over the release-site (Rennes). The advected air was unstable, with showers, some accompanied by thunder and squall-lines. Similar observations could be made from satellite pictures. The 12:00 UTC radio sounding of Brest showed a temperature profile which was unstable with respect to moist air, allowing the development of shower clouds up to about 28000 ft. Also the radio sounding of Paris showed an unstable atmosphere but with lower water vapour content. At both locations, the upper winds were Southwest and rather strong. The release started at 16:00 UTC.

24 October, 1994

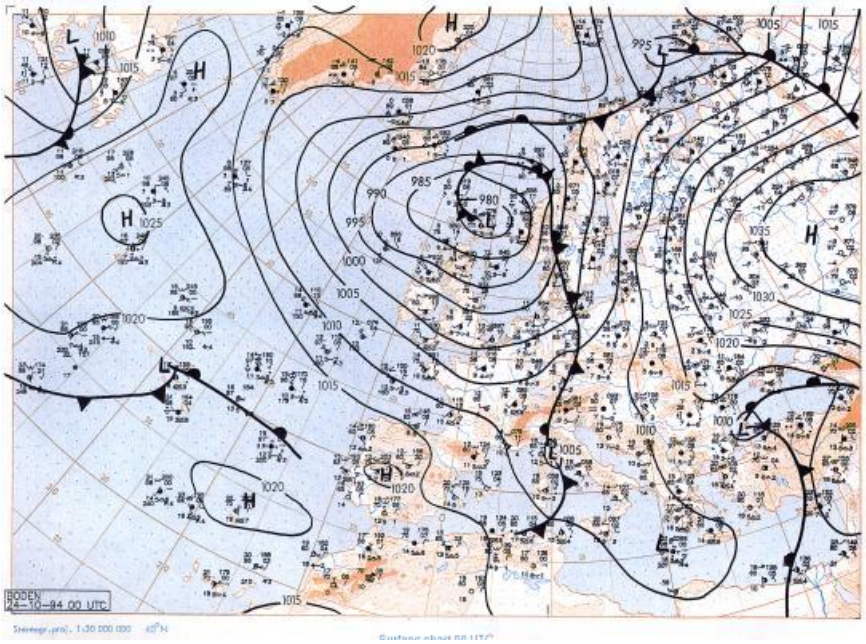

Figure 4 24 October, 1994, 00 UTC (ETEX web-site, 2019).

There was still an unstable flow over the release site and the advection area. However, because of the northerly movement of the controlling low over the North Sea, the wind in the advection area decreased. The expected cold front was to be seen south of Ireland.

25 October, 1994

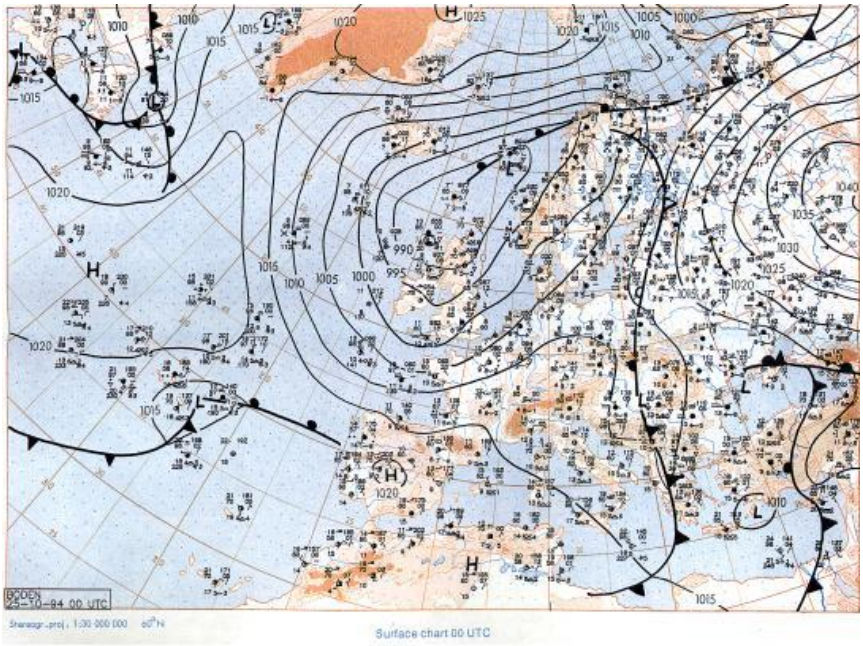

Figure 5 25 October, 1994, 00 UTC (ETEX web-site, 2019).

The further deepening of the mentioned cold front had not developed. The system was to be seen as a minor secondary low, at 52°N, 5°E. The cold front over The Netherlands, an instability front with showers, had the pressure pattern of a trough. The wind was backing more to the south with the approach of the front during the day, and after the passage of this front the wind was veering to the Southwest.

26 October, 1994

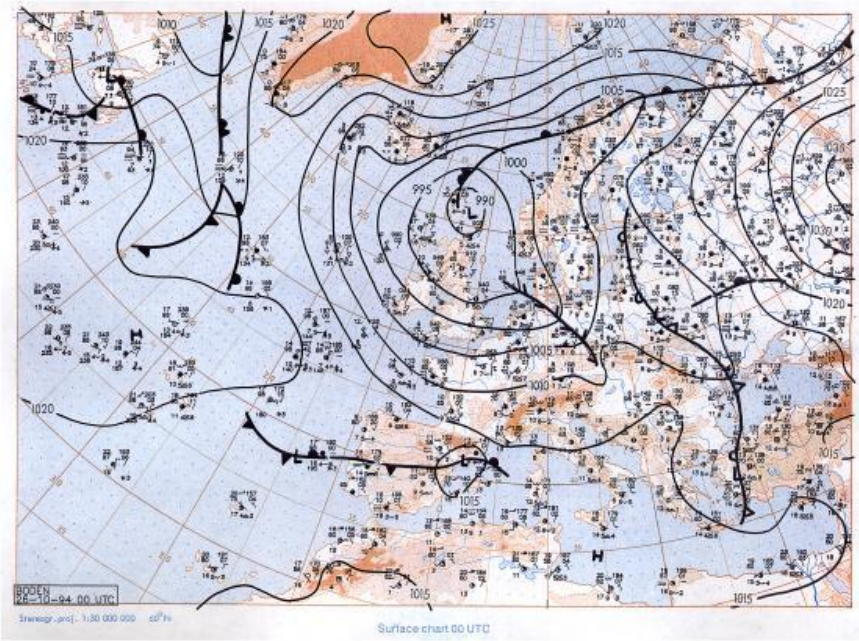

Figure 6 26 October, 1994, 00 UTC (ETEX web-site, 2019).

There was still a complex low-pressure system over the North Sea and Scotland. Shower weather with a wind tending to veer a bit over Western Europe towards west-southwest. The high-pressure cell over the Black Sea indicated that southerly winds could block any further movements of the tracer cloud towards the East.

Tracer release

Atmospheric tracers were released in the form of a homogeneous air stream containing a few percent of perfluoromethylcyclohexane (PMCH) tracer. The gas stream passed through a small chimney where the gas was released at the top.

The release started at 16:00 UTC on October 23, 1994, and lasted 11 hours and 50 minutes. 340 kg of the non-depositing inert gas PMCH (perfluoromethylcyclohexane) were released from Monterfil (48°03’30”N, 2°00’30”W) at an average flow rate of 8.0 g/s.

Results of DERMA

We here show preliminary results based on the different assumptions described in the method section. No method we have examined seems to be perfect for all cases, and therefore we instead show which results the different assumptions lead to.

All results are based on all available measurements, both non-zero measurements and non-detections. The time bins used have duration of three hours. The NUTS algorithm was run with 4 parallel chains for 2000 iterations in total, of which only the last 1000 iterations are used for sampling the posterior distribution to allow the chains to converge before the sampling starts.

First, we demonstrate the difference between including all time bins and including only the 50% bins that affect most measurements. Both results are obtained by assuming Gaussian likelihood.

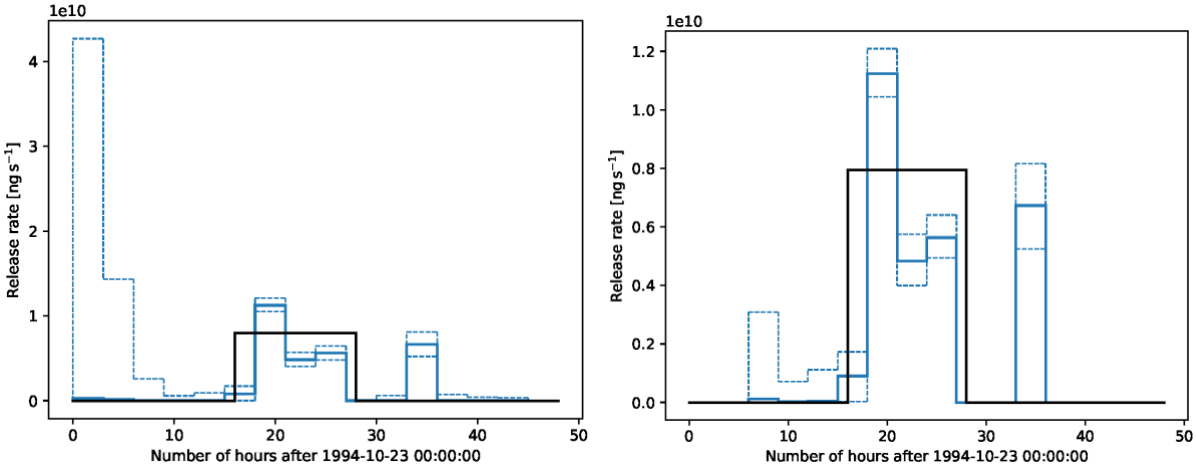

Figure 7 Left: including all time bins. Right: including the 50% bins that affect most measurements. Both results are based on the Gaussian likelihood. The solid blue line shows the median of the posterior distribution, and the dashed blue lines show the 5th and 95th percentiles. The black line shows the true release rate.

We see that the first few bins allow for a wide range of release rates, because the releases from these times are poorly constrained by the data.

Next, we compare the results obtained by assuming Gaussian likelihood and log-normal likelihood.

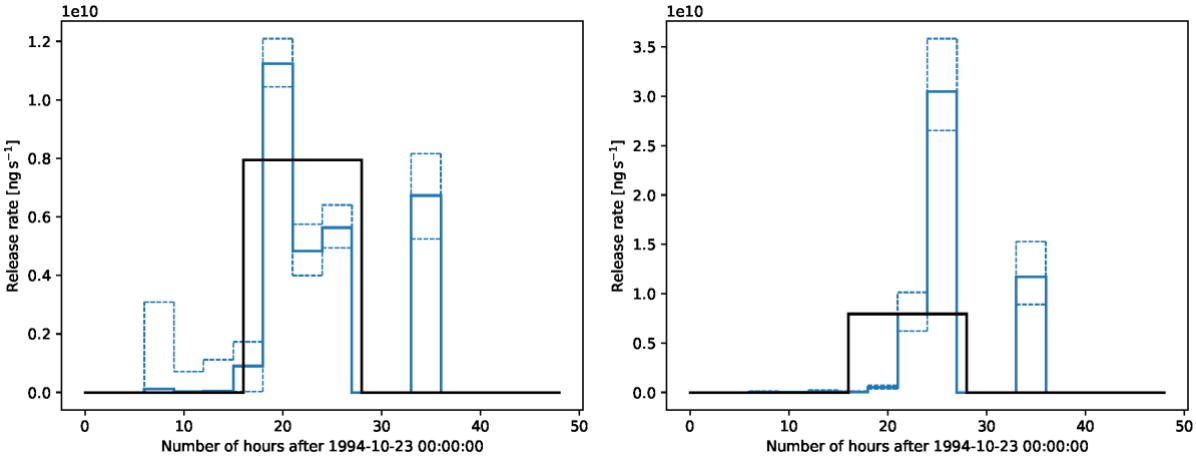

Figure 8 Left: Gaussian likelihood. Right: log-normal likelihood. The solid blue line shows the median of the posterior distribution, and the dashed blue lines show the 5th and 95th percentiles, respectively. The black line shows the true release rate.

In both cases, the main part of the release is estimated during the correct release period, but the timing and magnitude of the peak of the release differs slightly. Further, both approaches predict an additional release 5 hours after the true release ended.

Results of MATCH

This experiment was run with ERA5 weather data on 0.2 degree resolution covering the period 12URC 23 October to 00UTC 26 October, 1994.

A subset of 50 out of 930 non-zero observations were extracted by first restrict to observations valid after the release ended (9UTC 24 to 00UTC to 26, October). The subset was then extracted by so called weighted bootstrapping with withdrawal, that implies that a random selection will favour larger measured values, and that an observation only could be selected once. The very ten largest observation in the set were though explicitly selected to avoid being randomly excluded. Locations for the selected stations are shown in Figure 9.

The retrieved vertical source distribution is shown in Figure 10 (top) and total release rate (bottom). The timing of the retrieved release very much catches the true release period, although 86 kg of the release is retrieved less than the 340 kg in reported emitted. Anyhow the transport pattern is well caught as shown in Figure 11 andFigure 12. In Figure 1Figure 12 finally we present scatter diagrams for dependent and independent observations.

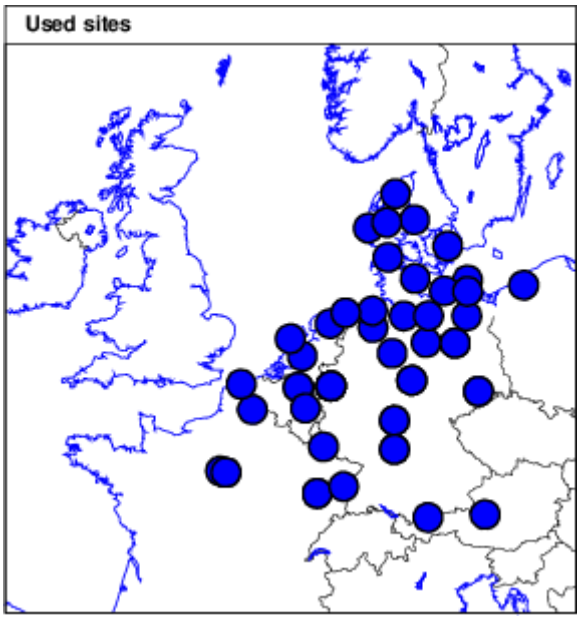

Figure 9 The sites for the 50 observations used for the source inversion.

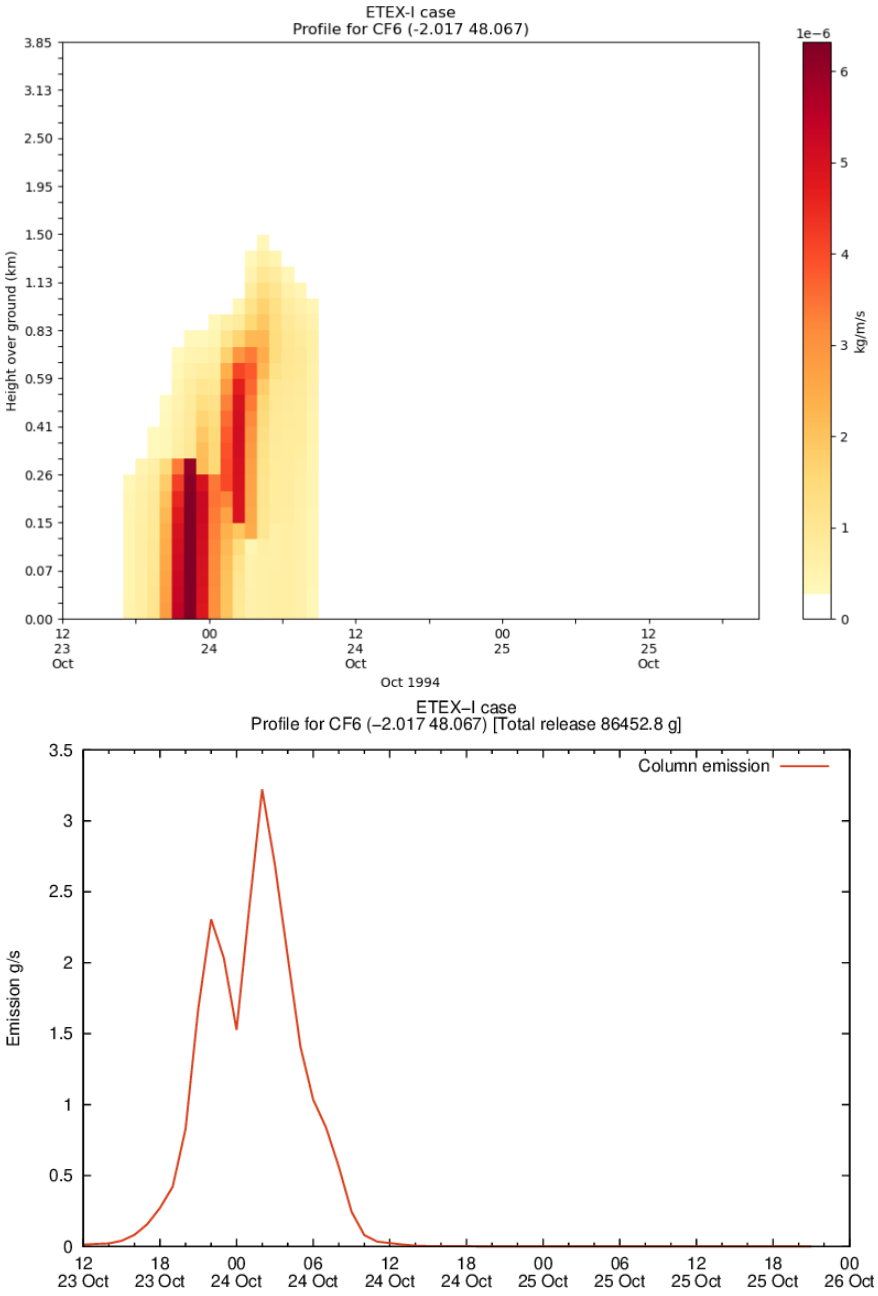

Figure 10 Retrieved source profile given as vertical extension (top) and emission rates (bottom).

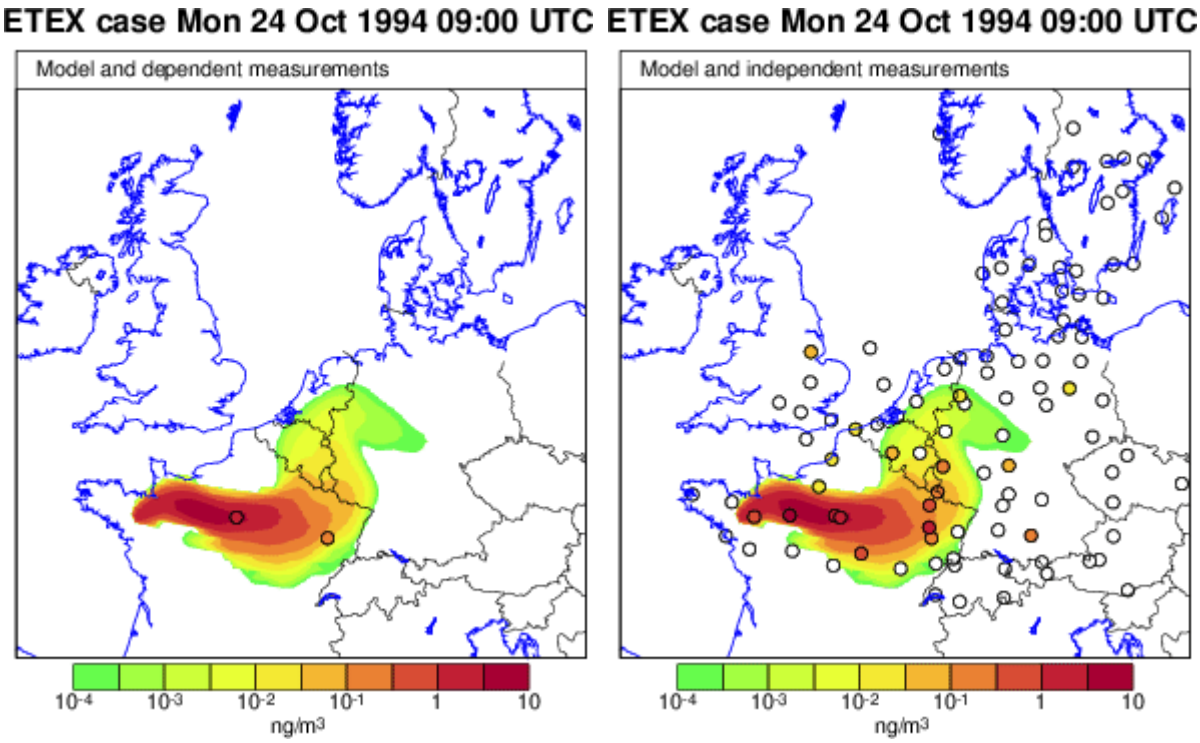

Figure 11 Assimilated ETEX-I plume at 09 UTC 24 October, 1994, together with the observations used (left) and all observations (right).

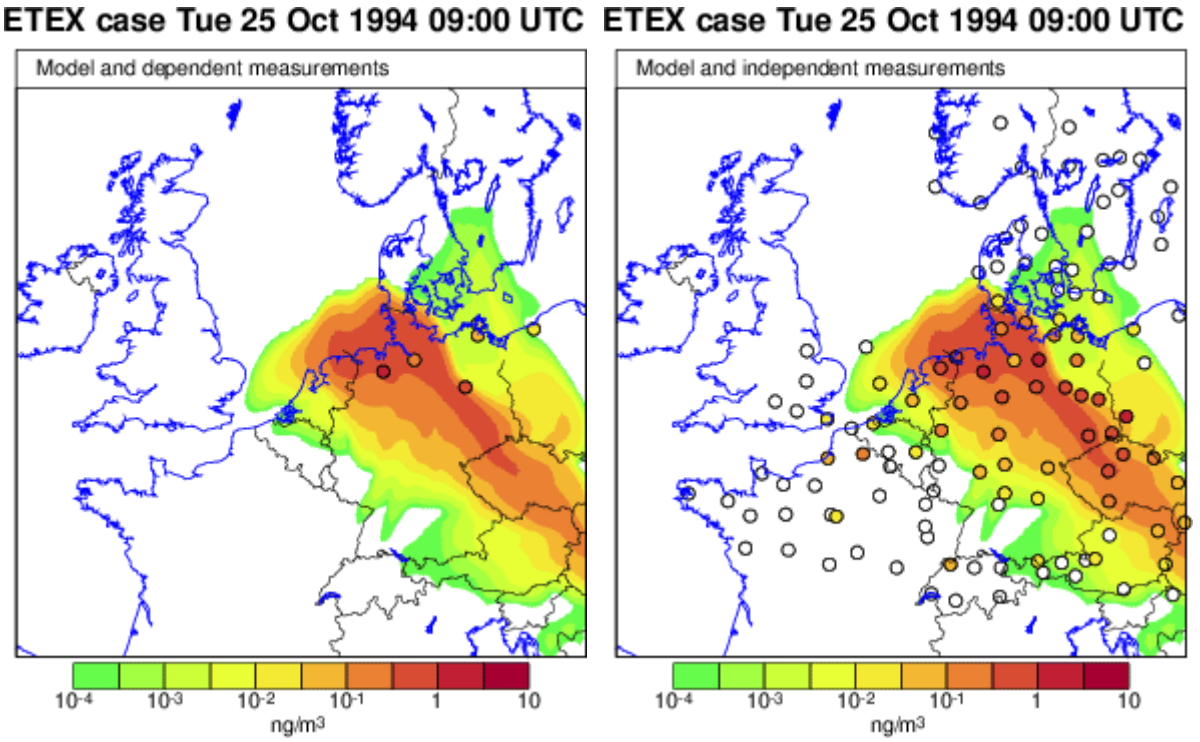

Figure 12 Assimilated ETEX-I plume at 09 UTC 25 October, 1994, together with the observations used (left) and all observations (right).

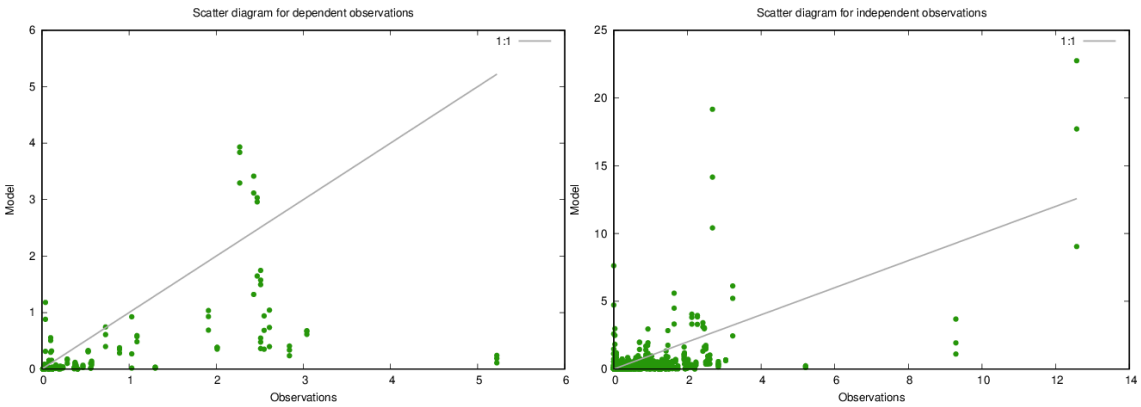

Figure 13 Scatter diagram observations vs. model for dependent observations (left) and independent (right).

Results of SILAM

The source retrieval of the emission of the ETEX experiment was performed through three scenarios that involved three different vertical emission profiles, set as 8-50 m, 8-500 m and 8-1000 m. For the simulations, ECMWF ERA5 meteorological data was used, with the resolution of the simulations being 0.125 degrees.

The regularization term was able to significantly reduce the noise of the retrieved source, as illustrated in Figure 14. The L-curve approach, where the regularization factor is selected based on the sharp angle of the curve, is shown in Figure 15. Although the retrieved temporal profiles of the three scenarios look similar, the estimated total emission rather strongly depends on the assumed vertical emission profile, as expected. However, in all three scenarios, the retrieved total emitted amount fell short of the actually released amount of tracer.

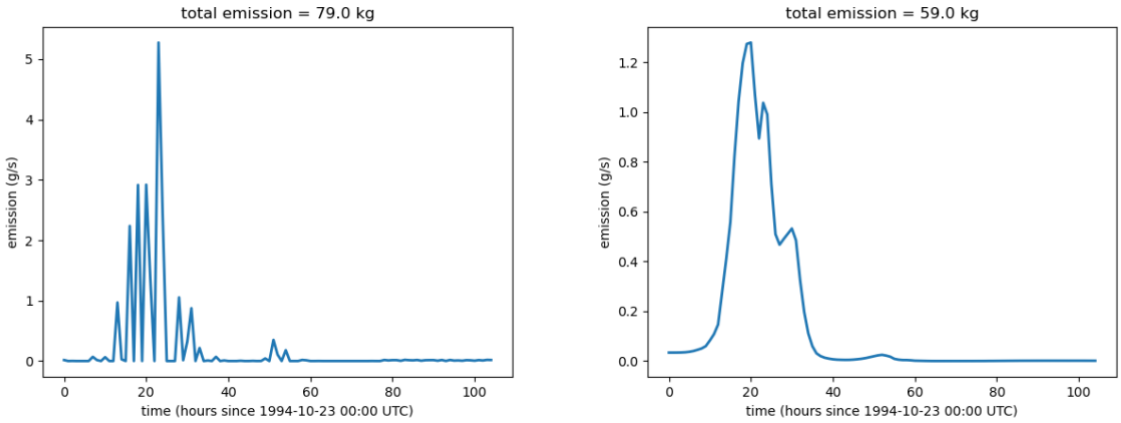

Figure 14 Retrieved emission for the vertical profile of 8-50 m with no regularization (left) and with regularization (right).

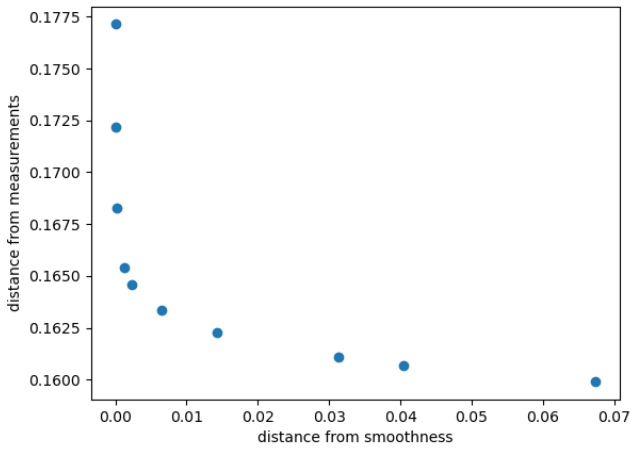

Figure 15 Illustration of the L-curve approach. The emission profile of the regularized case of Figure 14 is based on a regularization weight that corresponds to the bend of the curve.

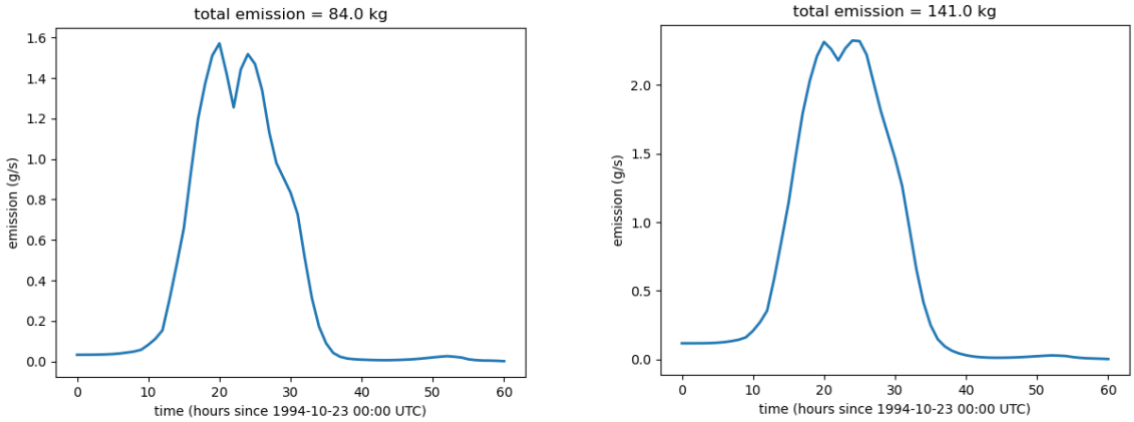

Figure 16 Temporal source profile for an emission elevation of 8-500 m (left) and 8-1000 m (right).

Results of SNAP

The release was assumed to occur between 1994-10-23 T00:00 and 1994-10-25 T12:00, with the release location of Monterfil with an atmospheric release radius of 1 m and a release height of 3-5 m. To determine the sensitivity to the number of non-detections the model was run using a penalty of $\sigma = 0.01$ for all non-detections, of $\sigma = 0$ for observations where the detected amount was $< 10^{-9}$ g/m^3, i.e. 100 times the detection limit, and without the penalty to compare the effects on the inversion.

Of the three model parametrizations, only one provides values of the correct magnitude as the actual released amount of PMCH (340 kg). The no-penalty approach only attributes a total of 5.6 kg of release material from the source. Setting the penalty term to value observations by a factor 100 ($\sigma = 0.01$) compared to non-detections increases the released amount to 11.8 kg. Removing observations below 10^{-9} g/m^3 (leaving 76 observations) gives a total of 394 kg of PMCH released and is in line with the true released quantity.

Comparing the release rate of the model to the true release rate shows the inversion method is prone to inserting much of the activity at the start and end of the actual release window, whilst the bulk of the release is not captured. Penalizing the non-detections inserts too much material

before the actual release window, with the complete removal of observations below 10^{-9} g/m^3 is more apt to insert too PMCH after the release window. The accumulated concentrations of PMCH are compared for the true source term and the source terms using no penalties in Figure 1Figure 18.

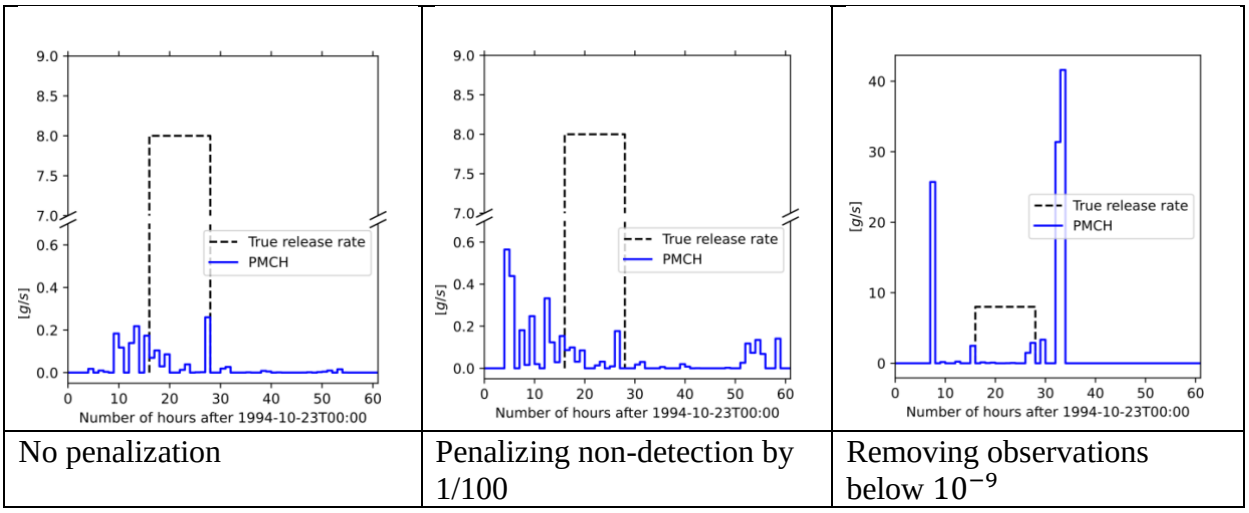

Figure 17 Release rate of PMCH during the ETEX inversion, with the true release rate in black using the SNAP inversion method.

Figure 18 Accumulated depositon of PMCH [g h/ m^3] of the forward run (left) and the source term from the inversion using all observations equally weighted (right). Triangles show the accumulated concentrations with white triangles marking no detections during the experiment.

The Autumn 2017 Case of Ru-106

During the period 3–6 October 2017, the Incident and Emergency Centre of the International Atomic Energy Agency (IAEA) was informed by Member States that low concentrations of Ru-106 were measured in high-volume air samples in Europe. The detected isotopes did not contain any other radionuclides (e.g. other fission products such as Cs-137) and were at levels far below those requiring public protective actions, however not accounting for the anticipated higher concentrations at the release site. Corresponding data and information were obtained from the IAEA (2017a, 2017b). The data comprise 387 measurements of Ru-106, some of which correspond to levels below minimum detectable activities. The data are time-average concentrations corresponding to varying time periods of up to seven days, cf. Figure 19 below.

From a meteorological point of view, seven days can be a long time with potentially a number of meteorological phenomena such as front passages taking placing at the release site within the period. Possible sampling scenarios include evenly distributed low concentrations at the station site throughout the sampling period, or brief high concentrations corresponding to a narrow plume passing over the site in a short while. Therefore, such measurement data should possibly be discarded in a localization study**.** The discarded data can, however, be used for verification purposes.

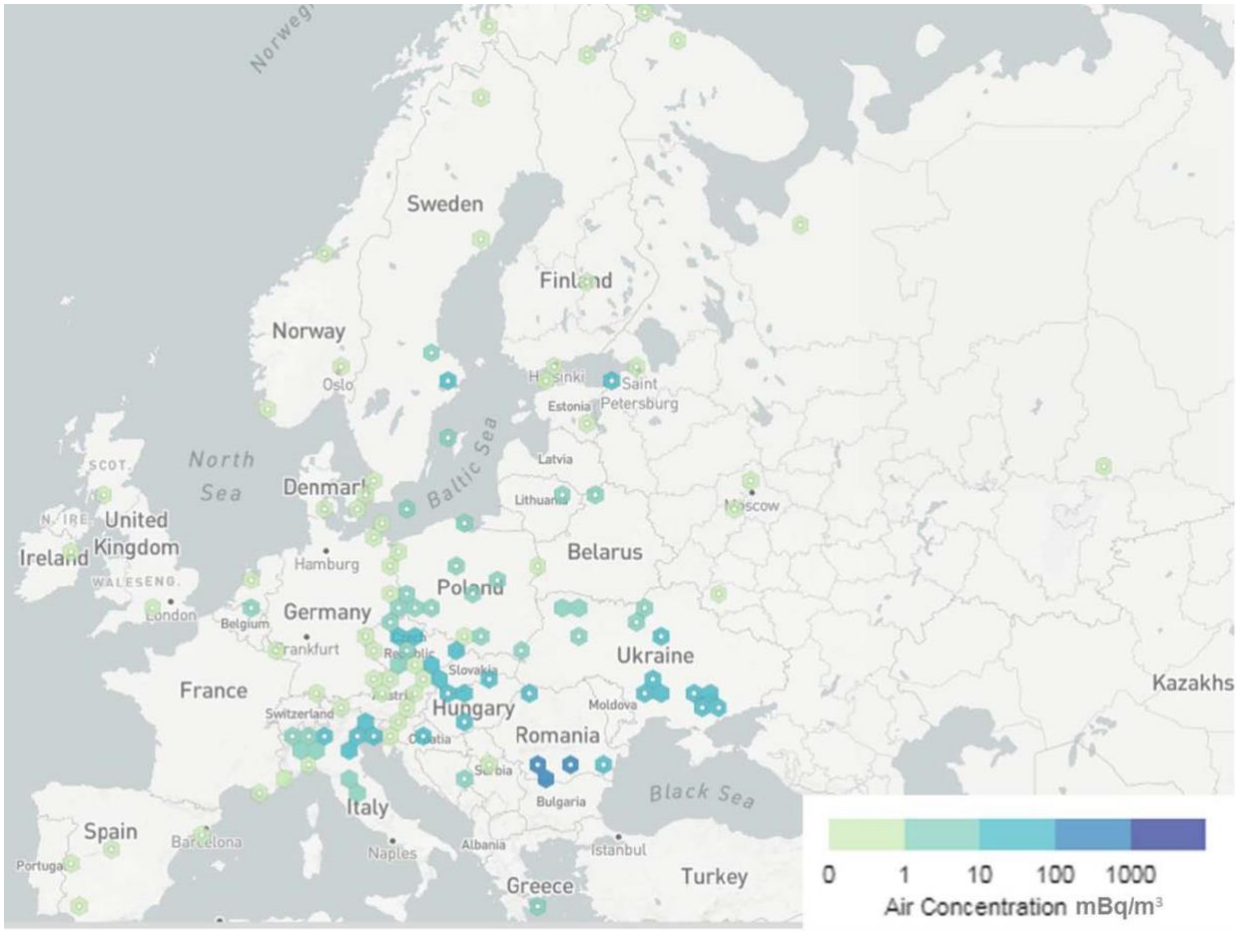

Figure 19 Locations where concentrations of Ru-106 in the air have been reported to the IAEA (IAEA, 2017a; 2017b). The measurements were taken during different sampling periods ranging from daily to weekly.

Results of DERMA

We again show our preliminary results based on the different assumptions described in the method section.

All results are based on all available measurements, both non-zero measurements and non-detections. Measurements were obtained from (Masson *et al.*, 2019). The time bins used have duration of six hours, and the source location is assumed to be the Mayak nuclear facility as suggested by previous studies e.g. by Tølløse *et al.* (2021). The NUTS algorithm was run with 4 parallel chains for 2000 iterations in total, of which only the last 1000 iterations are used for sampling the posterior distribution to allow the chains to converge before the sampling starts.

In the figure below, we compare the results obtained by assuming Gaussian likelihood and log-normal likelihood.

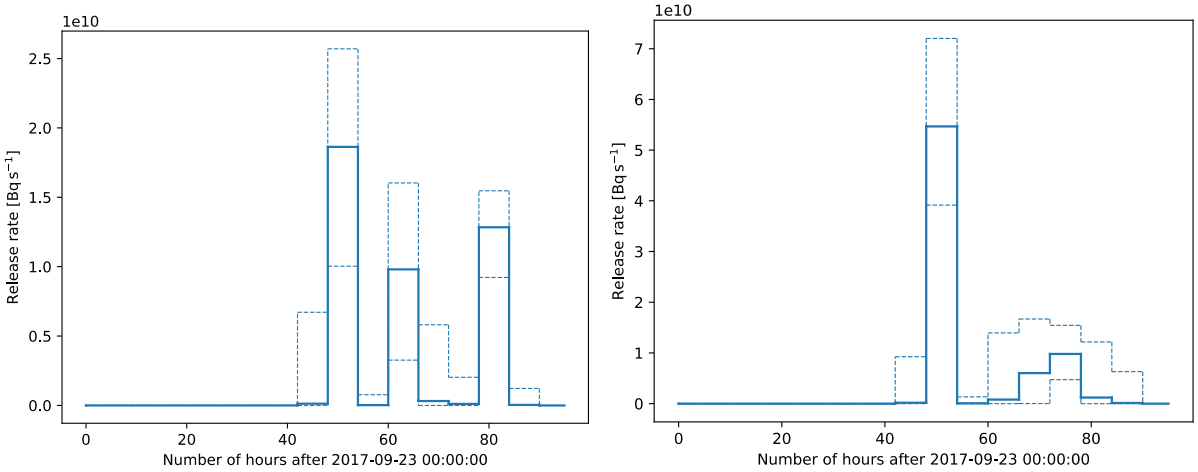

Figure 20 Left: Gaussian likelihood. Right: log-normal likelihood. The solid blue line show the median of the posterior distribution, and the dashed blue lines show the 5th and 95th percentiles, respectively.

Both results show a large peak after about 48 hours, which is around 0 UTC on September 25, 2017. Although there are some differences between the remaining parts of the two estimated release profiles, the overall period and the characteristic release rates are similar.

As mentioned previously, the results are quite sensitive to some of the assumptions made. Specifically, for the Ru-106 case, we found that changing the duration of time bins or including fewer or more time bins does change the resulting release profile somewhat. In the next part of the project, we will therefore focus on developing a better method for deciding which/how many time bins to include as well as what duration of time bins to use.

Results of MATCH

The met data used were IFS data on 0.2 degrees for the period 25 September to 5 October, 2017.

From out of 131 measurements with up to 36 hours sampling time a reduced set of 30 measurements were randomly selected by weighted bootstrapping (with withdrawal). The 10 largest measured values were taken before the random selection. Remaining measurements were used for validation. Figure 21 shows the sites for the selected measurements, and sites for validation.

The retrieved source profile for the Mayak location is shown in Figure 22 and Figure 23. The rather deep source may to some extent originate from long-range backward adjoint transport where the adjoint plume will be vertically distributed during the course of the transport. A total amount of 2e12 Bq is retrieved as total activity released.
Figure 24 shows scatter plots for dependent and independent observations. A rather good fit to independent observations as well is seen.

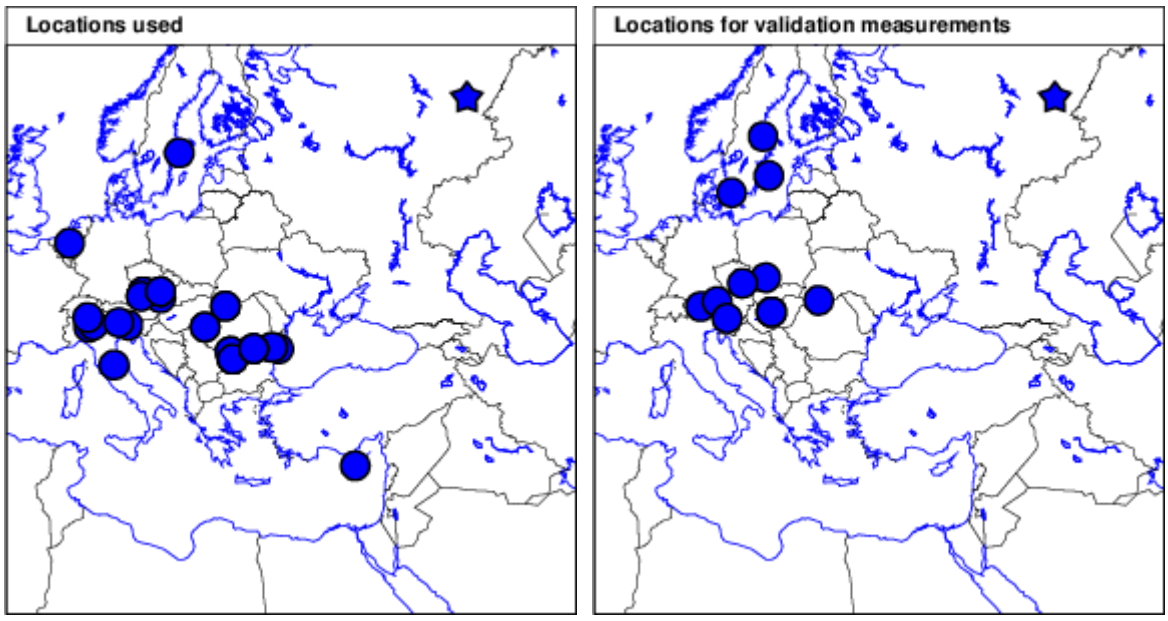

Figure 21 Sites for the reduced set of 30 measurements (left) and sites for validation measurements.

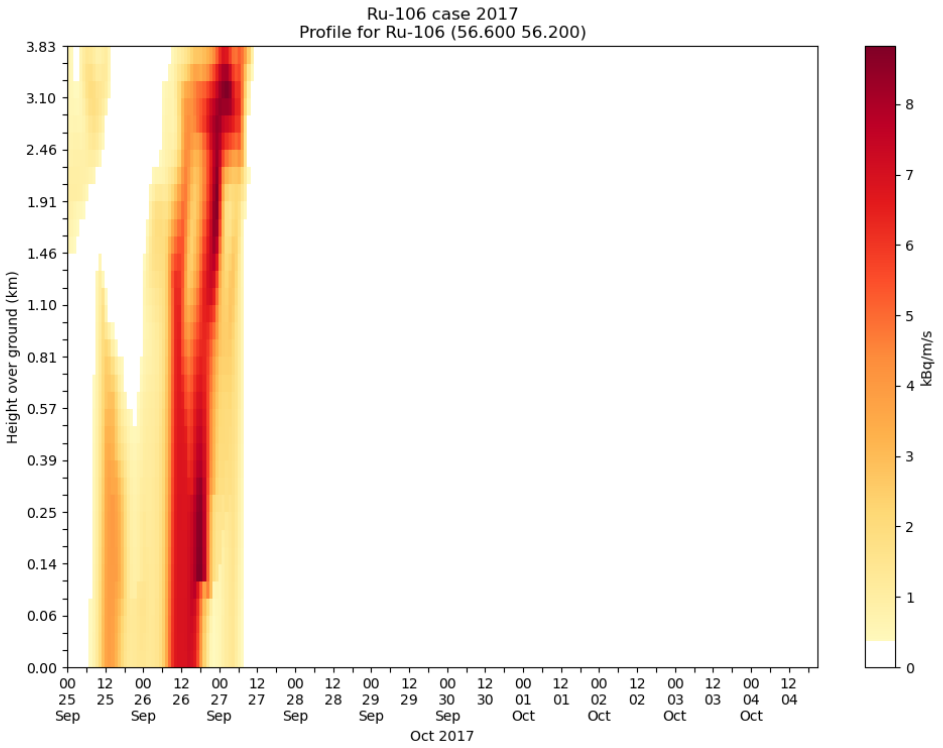

Figure 22 Vertical distribution of the source profile for the Mayak location.

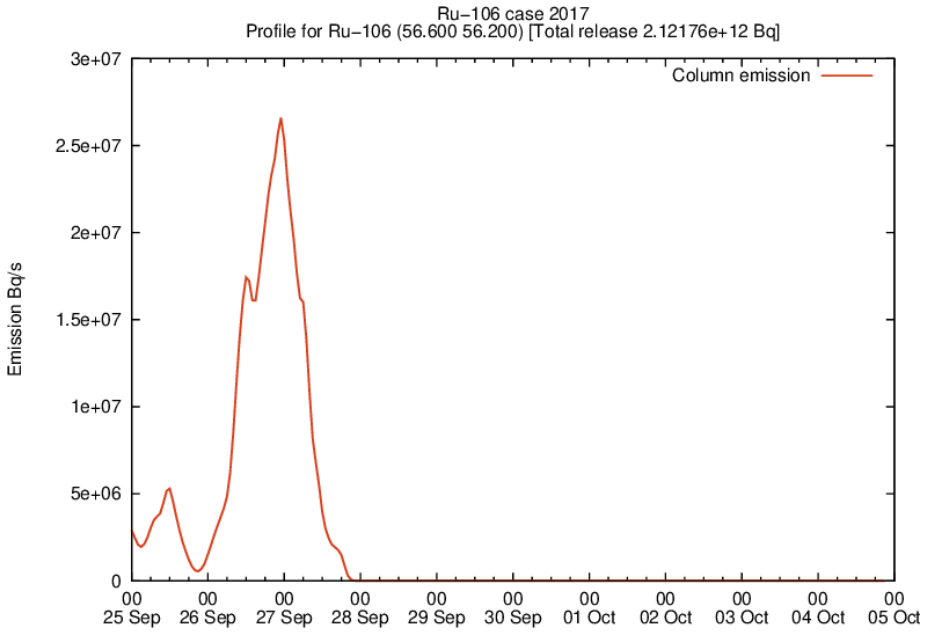

Figure 23 Temporal source profile for the Mayak location. A total estimate of 2e12 Bq release would explain the measurements used.

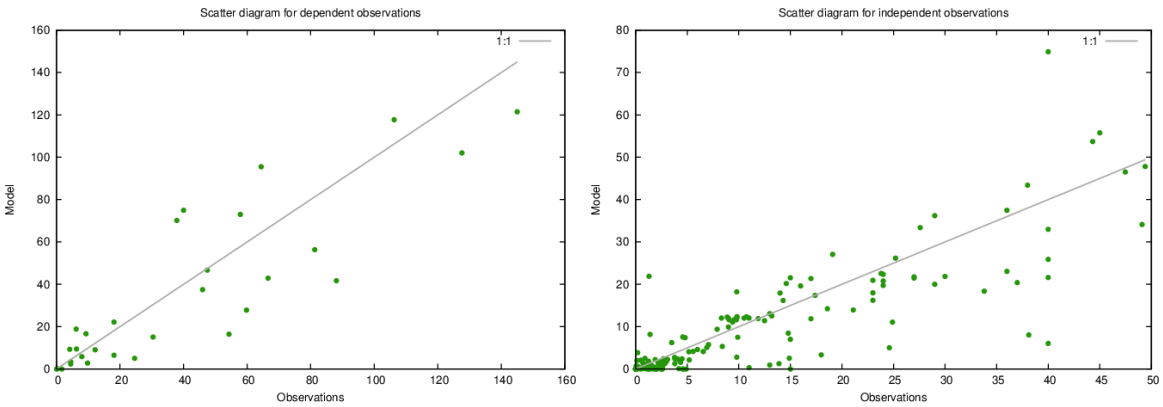

Figure 24 Scatter plots for observations vs model with dependent measurements (left) and independent measurements (right).

Results of SILAM

The SILAM retrieval of the source was performed using ECMWF ERA5 meteorological reanalysis data at a resolution of 0.5 degrees. The emission profile of the source was set to 0-500 m, and the emitted Ru-106 was set to consist of an aerosol with an effective particle diameter of 0.4 μm. Although all measurement points were used for obtaining the retrieval, later a subset of the points can be set aside for validation, similar to the MATCH results.

The retrieved emission profile was clearly peaked at September 24th, with a smaller peak on the second day. The smoothness of the emission resulted in the regularized and unregularized solutions are very similar. Here only the unregularized solution is shown in Figure 25, together with a scatter plot of the simulated versus measured Ru-106 concentrations. The total emission is estimated to be 3.5 x 10^{14} Bq.

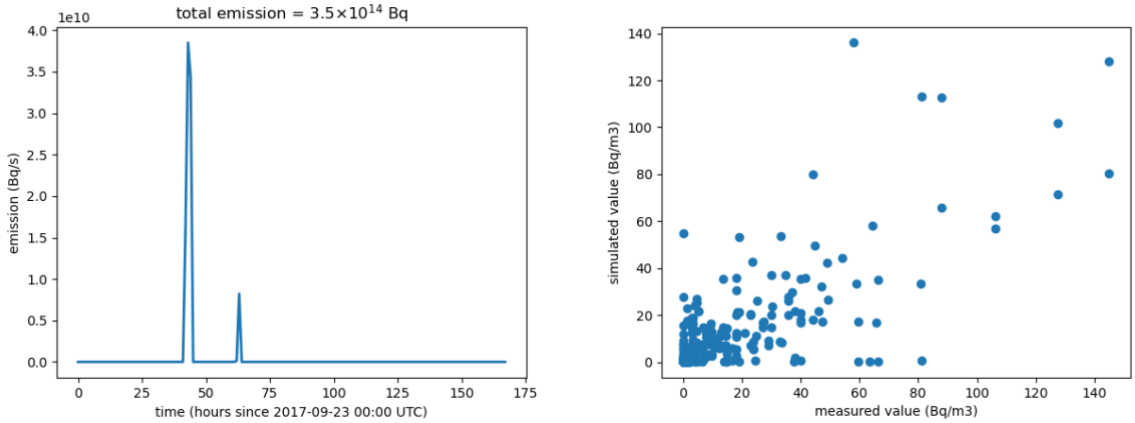

Figure 25 Retrieved temporal emission profile at Mayak from the SILAM model (left) and scatter plot of the measurements versus the model concentrations corresponding to the emission profile (right).

Results of SNAP

To investigate the source characteristics following the Ruthenium episode, the two likely release locations of Mayak and NIIAR as chosen. For both release scenarios the expected time of release was set between 2017-09-25 T12:00 and 2017-09-27 T00:00. To minimize the effect of non-detections and low observations lowering the total released, an inversion was performed penalizing observations below 0.1 Bq/m^3 (total 11 observations not penalized).

For the Mayak release location the total released activity was estimated at $5.2 \cdot 10^{12}$ Bq without the penalisation and at $2.0 \cdot 10^{13}$ Bq with the penalization of observations potentially under the limit of detection. Most of the release is contained in a peak at about 2017-09-25 T16:00, and suggest a single release episode with a duration of one hour or less.

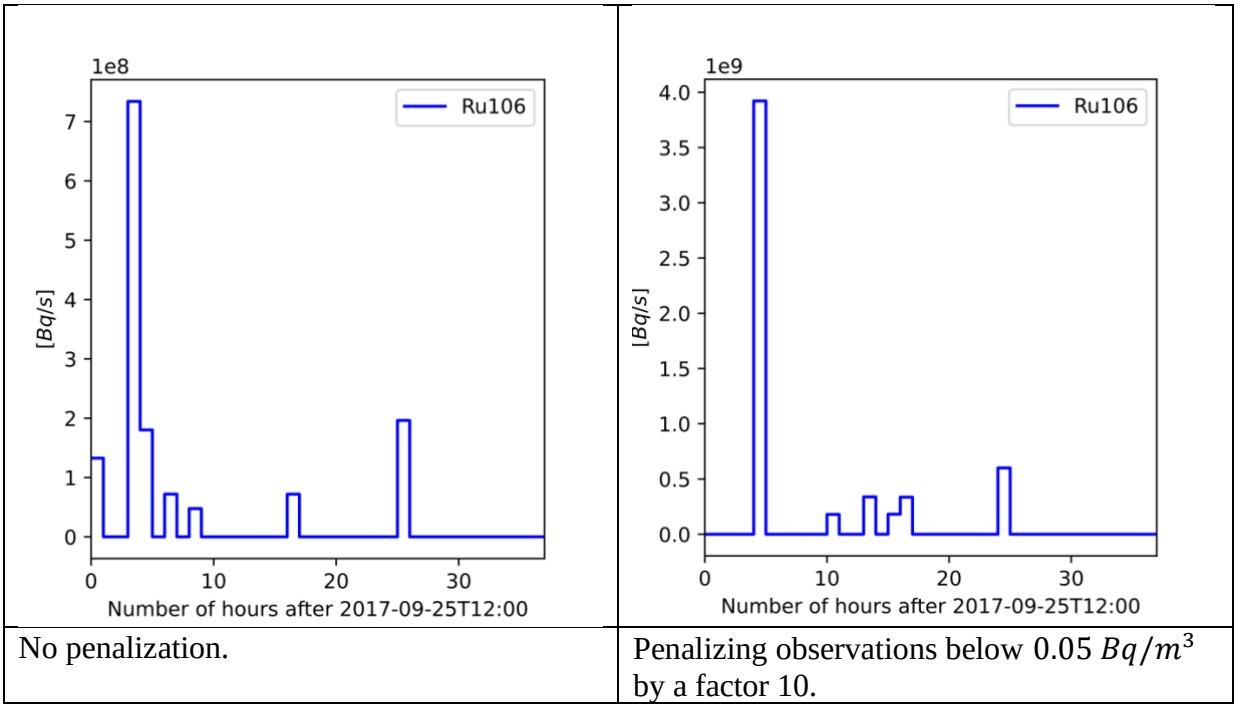

No penalization.	Penalizing observations below 0.05 Bq/m^3 by a factor 10.

Figure 26 Release rate from Mayak applying the SNAP inversion method.

For the NIIAR release location the total released activity was estimated at $9.3 \cdot 10^{12}$ Bq without penalisation and at $3.8 \cdot 10^{13}$ Bq with penalisation. In both cases the release is occuring as a peak at 2017-09-26 T02:00. Both Mayak and NIIAR show the same magnitude in total released activity, with NIIAR showing a later release time compared to Mayak.

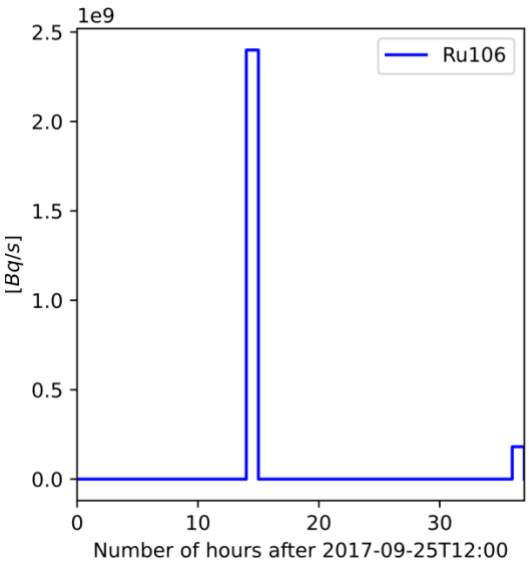

No penalization.

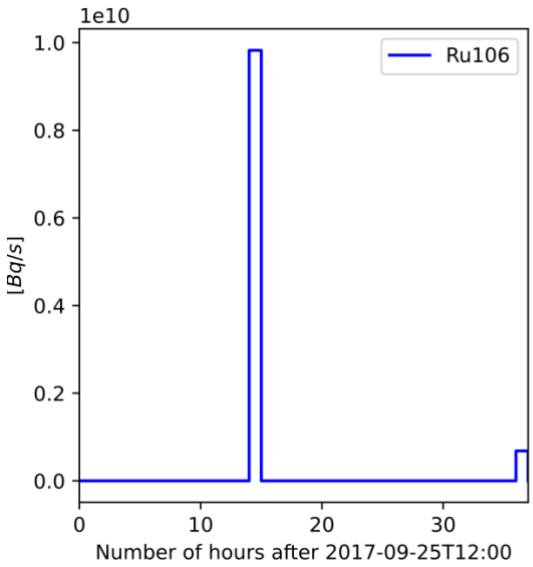

Penalizing observations below $0.05\ Bq/m^3$ by a factor 10.

Figure 27 Release rate from NIIAR applying the SNAP inversion method.

Artificial Case of a Release from the Loviisa NPP

A crude method was applied to select the most important nuclides to capture the pre-set of a large scale event by means of gamma dose rates at nearby gamma monitoring stations and national air filter stations.

The source term from which the selection of nuclides is derived is based on the outcome of calculated release sequence using the MELCOR computer code with an input deck for unit 4 at Ringhals NPP. The selected source term is a representative source term for a core melt event without functioning mitigation systems. The initial event is a total loss of all power systems without battery back-up, in addition to all steam-driven systems. Source terms from this type of event are connected with large uncertainties. Therefore, the selected source term is used to represent a large release for all Swedish nuclear power units in operation (see G*)*. The filtered containment venting system is assumed disconnected and instead comprise an exhaust pathway from the reactor containment. It was postulated that the exhaust pathway was open at the time of melt-through of the reactor vessel.

The MELCOR outcome (proportions of mass of the core inventory) has been translated into the accumulated released activity per nuclide including all 285 nuclides in the declared core inventory for unit 4 at Ringhals NPP. Almost 200 nuclides were selected and the released activity per unit of time was corrected for decay and ingrowth for the time period between the scram and the time of the release.

The time evolution is given in 1 hour time steps starting at the onset of the accident (time of the scram) and the following 12 hours, intended to represent the first part of release to undergo subsequent detection by the gamma monitoring stations and, if possible, capture by the air filter stations (see Figure 28 below).

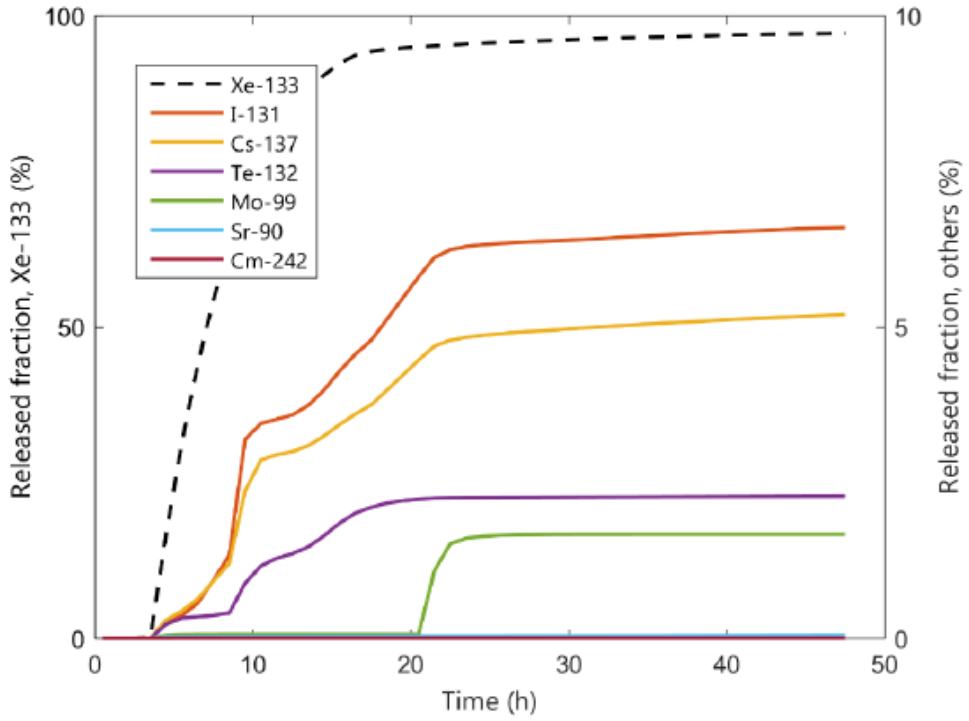

Figure 28 Released fraction of activity for selected nuclides in the case of a postulated event without functioning mitigation systems. Figure taken from Appendix 3 of Johansson *et al.* (2017).

The total dose rate at the gamma monitoring stations would reflect both the contribution from cloud and ground since the stations are not shielded from activity deposited on the ground. Over time the contamination of the station itself would also contribute to the measurement. The accumulated activity per nuclide for the 12 hour time period was multiplied with the nuclide specific cloud dose gamma factor, values taken from Eckerman and Leggett (2013). Here, no considerations were made regarding the differences among the amount of released nuclides subject to dispersion and plume depletion during the transport from release to the station. Furthermore, no corrections were made for decay and ingrowth during the plume transport as implied by the crude methodology employed. The accumulated released activity was multiplied with the nuclide specific ground deposition gamma factor (Eckerman and Leggett, 2013) for all nuclides except noble gases as a rough approximation for the ground contribution); the ground deposition gamma factors selected are those for 1 cm soil entrainment to simulate surface roughness.

The accumulated released activity for the 12 hour time period, excluding the noble gases, was combined with the information on the energy and yield (i.e. photon energy per nuclide transformation for each nuclide (Eckerman and Ryman, 1993) as a first approximation) to mimic the air filter station signals. No account was taken for decay and ingrowth for the period of time between the capture of the release in the filter and the subsequent gamma detector measurement.

Based on the investigation, a set of 11 nuclides was chosen to represent important nuclides: Kr-88*, Xe-133*, Xe-135*, Xe-135m*, Cs-134$^{\#}$, Cs-137, I-131$^{\#}$, I-132*$^{\#}$, I-133$^{\#}$, I-135$^{\#}$ and Te-132. The list consist of top 5 for the gamma monitoring station (denoted with *), top 5 for the air filter stations (denoted with $^{\#}$) representing more than 90% of the dose rate contribution in the first 12 hours of the postulated event with the crude methodology employed. Moreover, two nuclides from the top 10 list, Cs-137 and Te-132, were included since they represent key nuclides as seen from historical releases.

The artificial scenario consisting of simulated filter station and gamma station measurements was derived by predicting the atmospheric dispersion of radionuclides from a 9-hour release at the Loviisa nuclear power plant starting at 8 UTC on 2021-09-22. The FMI atmospheric dispersion model SILAM was applied to the release scenario described above using Harmonie NWP model forecast data of 5 km horizontal resolution and hourly time resolution thereby providing 48 hours of hourly average concentration values at filer stations and gamma doses at gamma stations by using the gamma dose model described above in section Semi-infinite Gamma Dose Model. Note that in a real case, the filter stations are likely to measure average concentrations at longer time periods, e.g. 12 or 24 hours, or even a week.

By using the artificially generated filter station and gamma station data, the task for the atmospheric dispersion models now is to estimate the time profiles of the release of the various radionuclides detected by the filter stations involved.

Results of DERMA

As described in the method section, we have only included the filter station measurements for this case. We used the instantaneous concentration values at the locations of the five available filter stations to compute averages over 12 hours. We then use these 12 hour averages as synthetic concentration measurements. If the average concentration is below the threshold value 0.1 mBq/m^3, the measurement is interpreted as a non-detection. The time bins used

have duration of three hours. The NUTS algorithm was run with 4 parallel chains for 2000 iterations in total, of which only the last 1000 iterations are used for sampling the posterior distribution to allow the chains to converge before the sampling starts.

Because we ignore gamma measurements, the amount of data is very limited for this case, and the release is therefore not very well constrained for most time bins.

In the figure below, we compare the results obtained by assuming Gaussian likelihood and log-normal likelihood. As an example, we show the result for the radionuclide Cs-134; the results for the remaining particles look very similar. The release profiles for the noble gasses, on the other hand, cannot be determined before we include the gamma measurements. These will be included in the next part of the project.

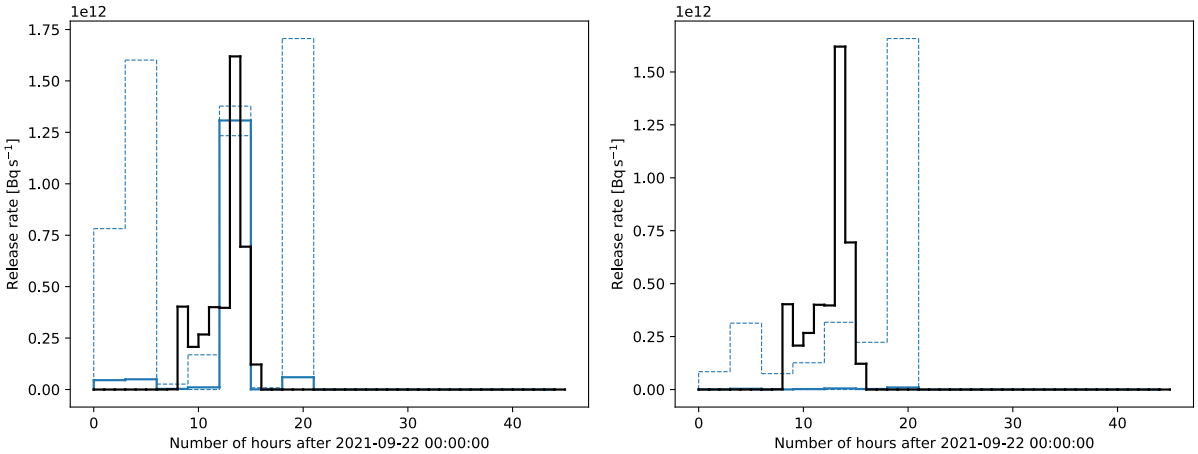

Figure 29 Left: Gaussian likelihood. Right: log-normal likelihood. The solid blue line shows the median of the posterior distribution, and the dashed blue lines shows the 5th and 95th percentiles, respectively. The black line shows the true release rate.

For both results, it looks like the release from most time bins are not properly constrained by the data. This may indicate that more time bins should have been excluded from the analysis, or that more measurements are needed. Further, the release profile predicted by the log-normal distribution does not really resemble the true release. It should be noted, however, that when using the log-normal likelihood for this case, the algorithm does not converge, and hence the result cannot really be interpreted as a probability distribution. This indicates that there is not enough data to use the log-normal distribution with this dataset. For the Gaussian likelihood, on the other hand, the estimated release from 12 to 15 hours is reasonably well constrained by the data, and this seems to capture the magnitude of the release quite well.

Results of MATCH

The met-data used for this case is operational IFS data on rotated lat-long grid with 0.1 degree resolution.

We retrieved the source profiles from both synthetic filter data and modified gamma doses at EURDEP locations. For the filter station we used all hourly provided data. while we for the gamma doses we first only considered measurements above 5 micro Sv/h and then made an extraction to 50 measurements by weighted bootstrapping. Figure 30 shows the sites used in the both cases. A bit though odd to find gamma dose sites over the Finish bay.

For retrieval of nuclides from gamma doses we assumed three nuclides, I-132, Kr-88 and Xe-135, to be the dose carrier. In the following we present retrievals of Kr-88 as one nuclide appearing in both data sets. A complicating factor is that the modelled gamma doses only consider air cloud contribution while the observed gamma doses may also include ground shine.

We found some issues regarding filter data where the Kotka site dominates the scene and very much defines the solution. Moreover, we had to slightly move the Loviisa power plant somewhat to the east to got hit by the adjoint plume from Kotka. The Figure 31 shows the retrieval of Kr-88 profile using filter data. The retrieved release considering Kr-88 is here in between 12 and 18 UTC 22 September, 2021, with the total activity released for this nuclide of about 1.8e16 Bq.

To illustrate the dominance of Kotka for the filter data, Figure 32 shows the retrieval where Kotka is left out. The signal does then mainly arise from Kiruna and Umeå filter stations. The retrieved emission profile is in time about 12 hours earlier and with significant lower total activity released.

The retrieval of the release profile of Kr-88 derived from gamma dose measurements is shown in Figure 33 where the release is proposed to be lasting from 12 UTC 22 September to 06 UTC 23 September. Here the three nuclides I-132, Kr-88 and Xe-135 are proxy for the nuclides not included. The retrieved total activity of Kr-88 is then amplified in relation to the filter data to 1.4e17 Bq. The retrieved activities released for I-132 and Xe-135 are 2.2e17 and 3.0e16 Bq, respectively, that in total lead to 3.8e17 Bq.

Figure 34 show scatter diagram of gamma doses for observations vs model with dependent and independent observations. The dependent the model does fairly well for lower magnitudes of the data while some high observations are not included in the source inversion. For independent observations the scatter is not all to convincing. The modelled gamma doses only consider air cloud contribution while the observed gamma doses also included ground shine.

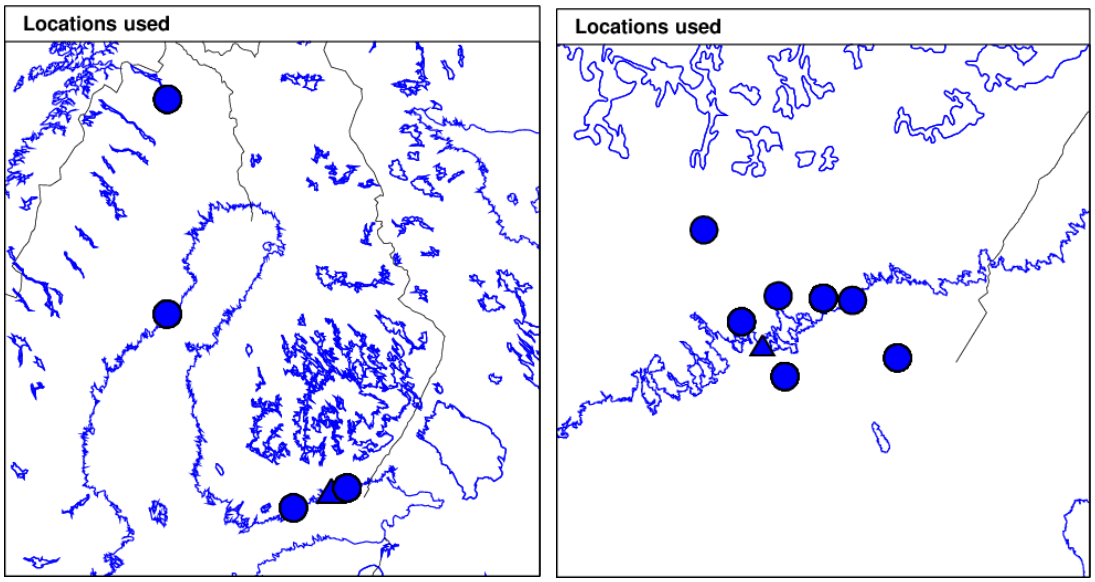

Figure 30 Locations for filter station data (left) and for gamma dose data (right). The Loviisa NPP location is plotted with a filled triangle.

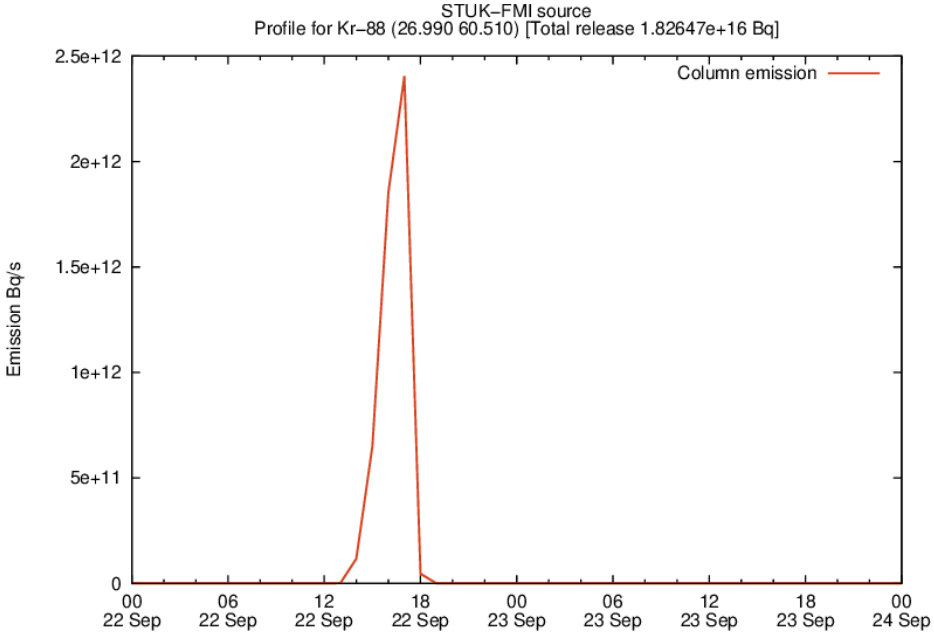

Figure 31 Retrieved source profile for Kr-88 with filter data for Loviisa NPP showing a rather short emission pulse.

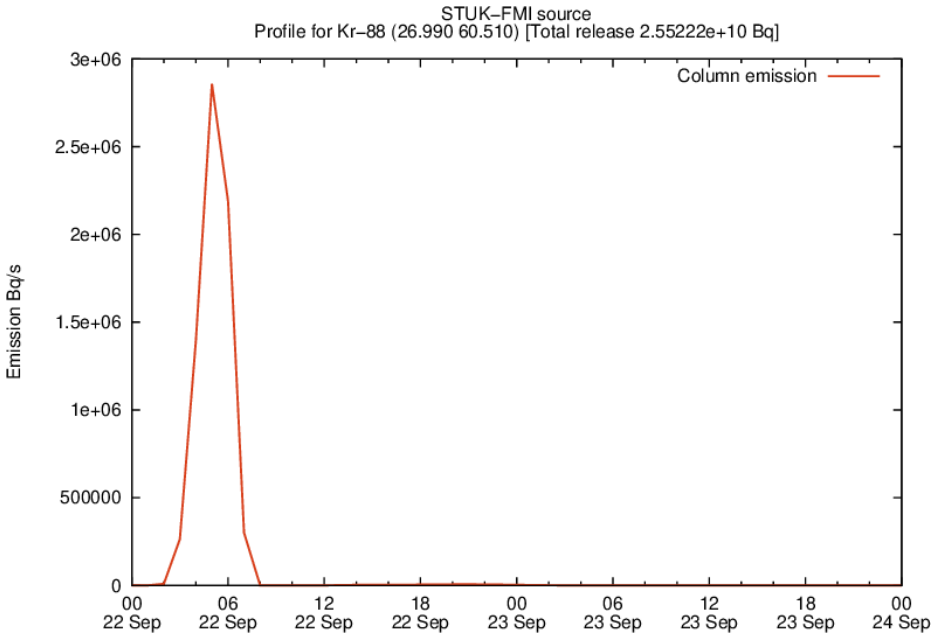

Figure 32 Retrieved source profile with **filter data** for Loviisa where the site Kotka is excluded. The retrieved profile is shifted somewhat earlier than in the retrievals above, and with significant lower total activity.

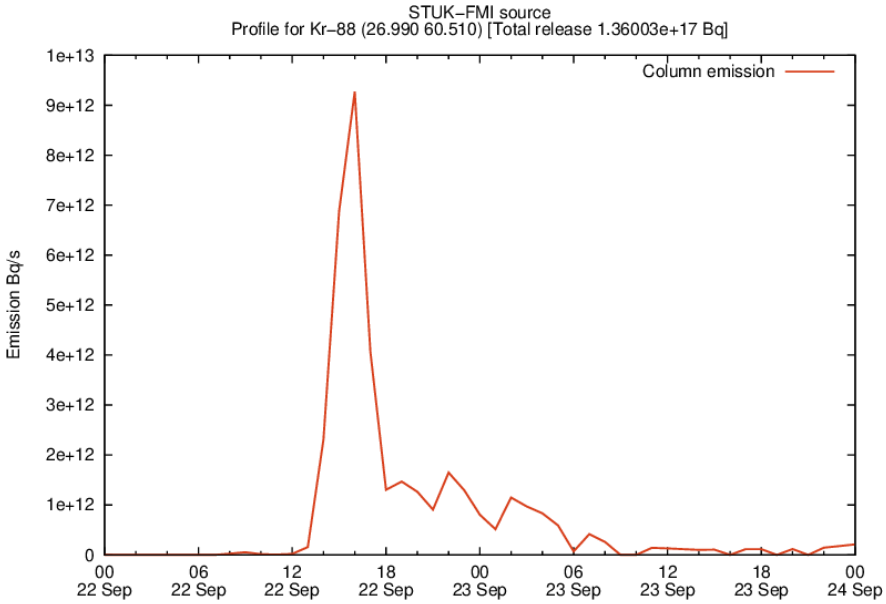

Figure 33 Retrieved source profile for Kr-88 using gamma dose measurement and I-132, Kr-88 and Xe-135 as dose carriers.

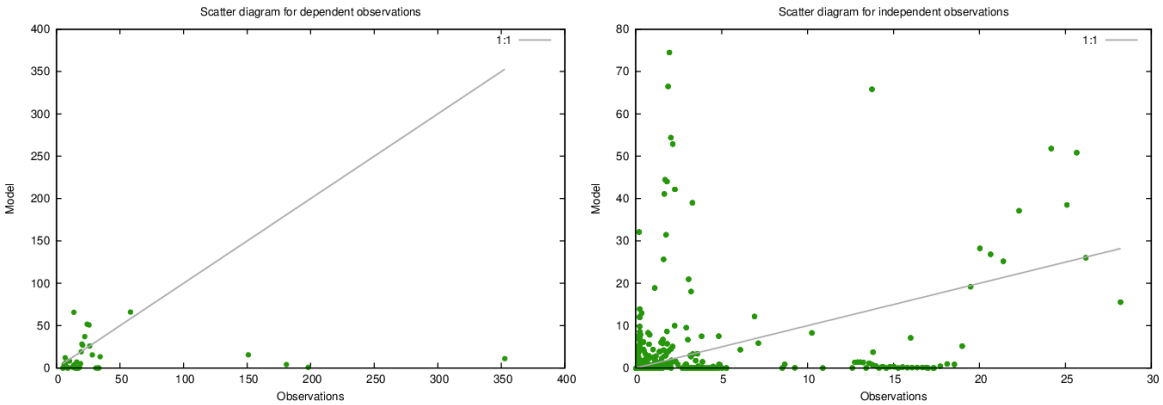

Figure 34 Scatter diagram for gamma dose observations vs model gamma doses for dependent observations (left) and independent observations (right).

Results of SILAM

The source characterization of the simulated accident was tested using the simulated dose rate observations only. The source characterization was performed with operational IFS meteorological data, and at a resolution of 0.125 degrees. The emission was set to occur evenly at an elevation of 0-200 m. The SILAM dose rate result consisted of the sum of the dose rates from the in-air and deposited concentrations of the nuclides. A background dose rate of 0.1 μSv/h was added to the SILAM results. Half of the emitted nuclides of the original simulation of the accident, i.e. I-131, I-132, Kr-88, Cs-137, and Xe-135 were selected as dose rate carriers, emitted evenly.

The source characterization was greatly restricted by the dose rate from the emitted plume not hitting the same stations as in the simulation of the accident. The problem is likely related to the dissimilarities of the meteorological data, as the MATCH simulations with the same meteorological data experienced similar results, and as the original simulation was performed with the same SILAM model as the source characterization. Despite a basically zero correlation with the simulated measurements, a clear emission peak was still found by the retrieval, as shown in Figure 35.

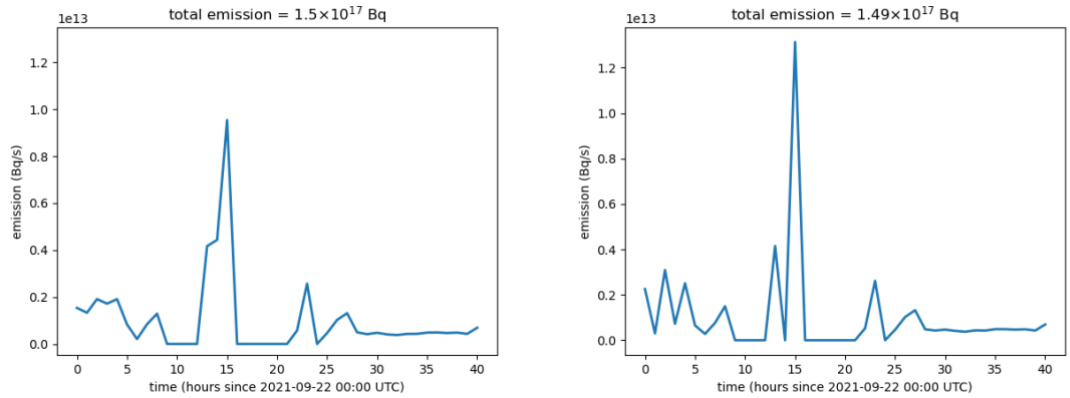

Figure 35 Retrieved profile of the emission at Loviisa NPP from the SILAM model. Left: regularized solution, right: unregularized solution.

Results of SNAP

The Loviisa case was assumed to release radionuclides between 2021-09-22 T00:00 and 2021-09-23 T00:00. Although gamma measurements may be added to the linear system, this extension was left as a future extension. The temporal release rate is unfortunately not modelled adequately by the inversion, and the source term appears chaotic. Manual exclusion of stations shows a great dependence on singular stations, and there are only a limited number of observations which can be used for constraining the release.

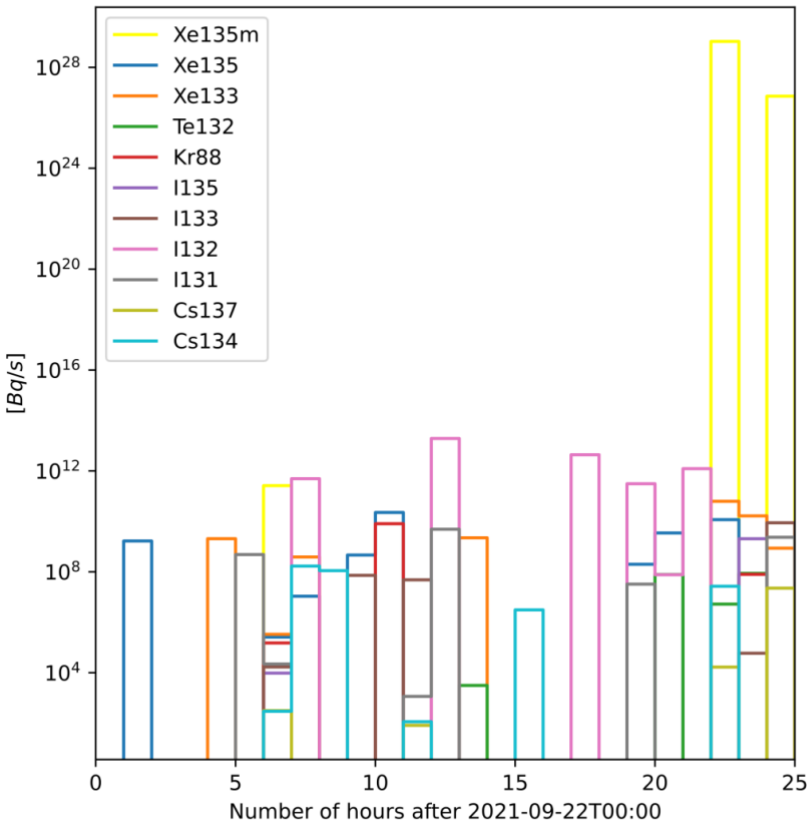

Figure 36 Temporal release characteristics for Loviisa using the SNAP inversion method.

ARGOS and Source Characterization

The Long-Range dispersion model interface in ARGOS has been developed in close cooperation with the different model providers through a number of years. The default interface is capable of handling forward deterministic Atmospheric Dispersion Modelling. As well specific interfaces has been developed for specific modelling needs such as handling ensemble calculations (developed in cooperation with DMI) and Adjoint modelling results (developed in cooperation with SMHI and SSM). Likewise, new interfaces will have to be developed in order to handle Source Localization (SL) as well as Source Characterization (SC) based on various measurements of radionuclide air concentration and gamma doses. The implications of such interfaces will be discussed in this section.

Concentration Measurements in ARGOS

The ARGOS-DSS features several different options for visualising different kinds of radiological measurements. An example is shown below where a plot of European Monitoring Stations is presented in ARGOS. Station data are imported using the EURDEP-protocol, see Figure 37.

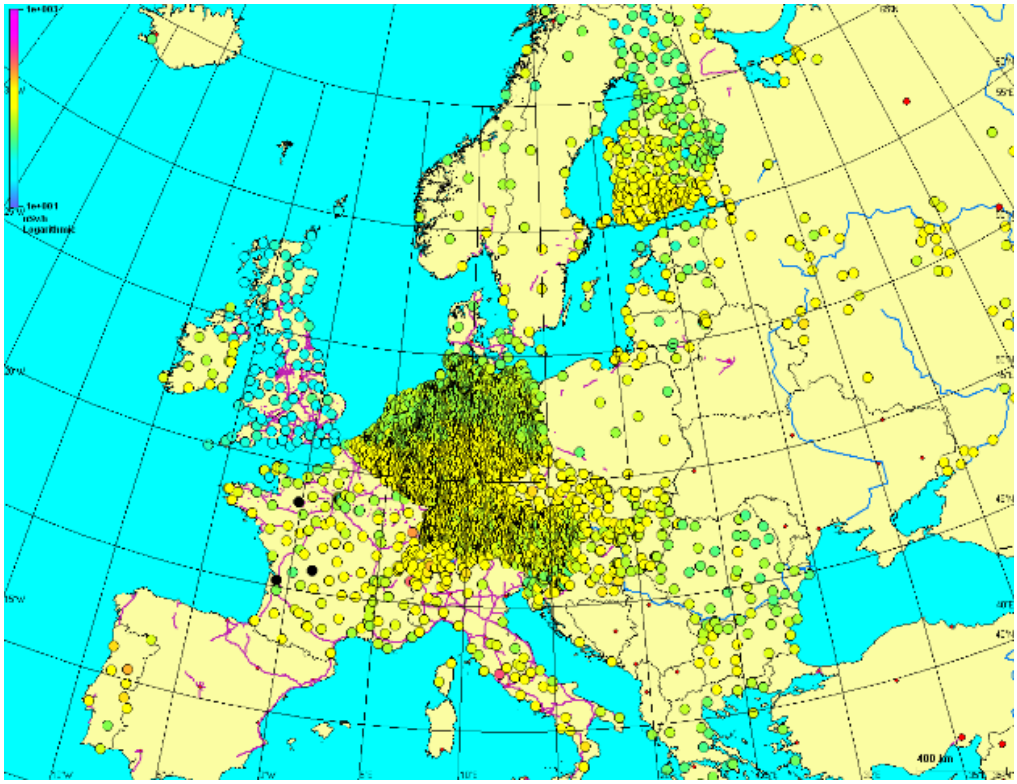

Figure 37 European Monitoring Stations presented in ARGOS.

The typical output from these types of Permanent Monitoring Stations is a dose rate; normal unit µSv/h.

Likewise, ARGOS is capable of importing and presenting data from Air Sample Stations – again importing data using the EURDEP-protocol. Typical output from these Air Sample Stations is an air concentration; normal unit Bq/m^3 (per nuclide).

Request for Source Characterization Calculation from ARGOS

The existing Request dialog in ARGOS today is focused on doing forward Atmospheric Dispersion modelling; giving the user options for selecting a release point (a reactor) and a release description (source term – or ensemble of source terms) and a release time, see Figure 38.

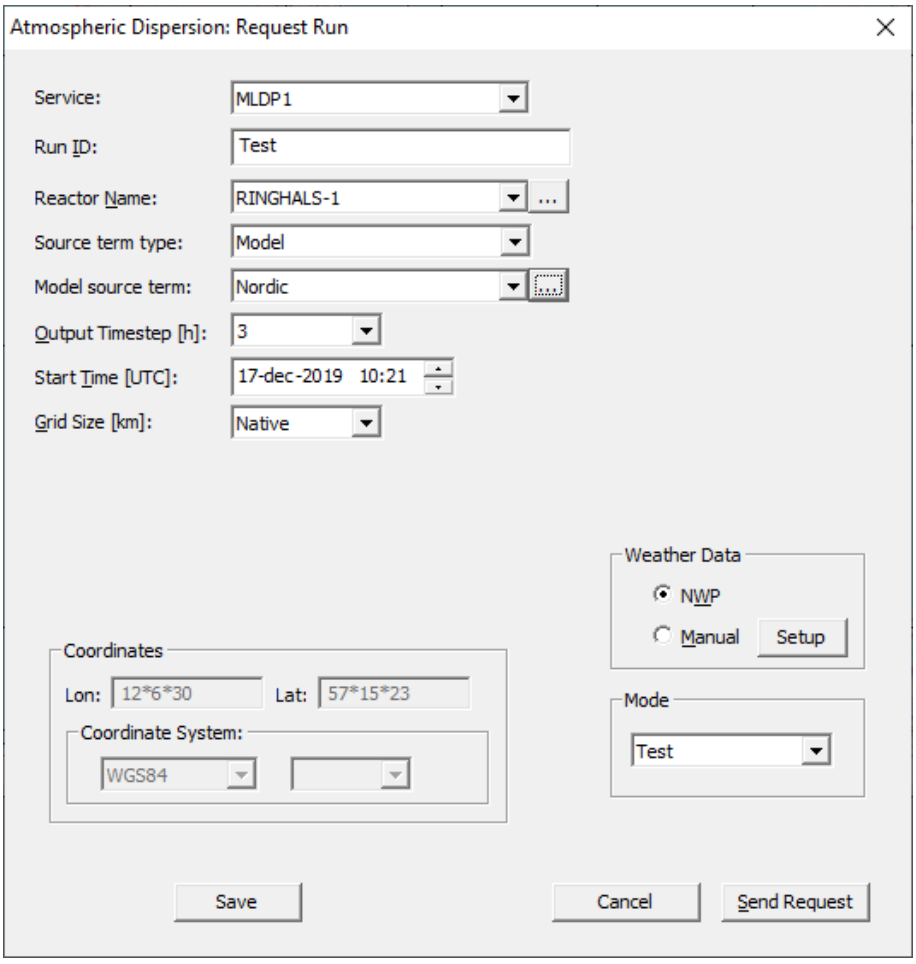

Figure 38 Forward atmospheric dispersion modelling request dialog in ARGOS.

For Source Localization and Characterization the needs are quite different from (normal) forward ADM. The user needs to provide a (number of) detection(s) of time-average air concentrations to be part of the request sent to the model, and for source characterization potentially also gamma measurements. As ARGOS already today have a module for presenting different measurements in the system (see section above) it would be natural to base the GUI for requesting SL or SC on the existing GUI for selecting measurement data to be visualized in the system. Due to the number of different types of measurement data, the GUI for selection is rather complicated, see Figure 38.

The needs for SL and SC can be narrowed down to these three parameters:

- The area of interest – the area from which the system should select measurement data
- The time frame of interest – the time period from which the system should select measurement data
- The type of measurements

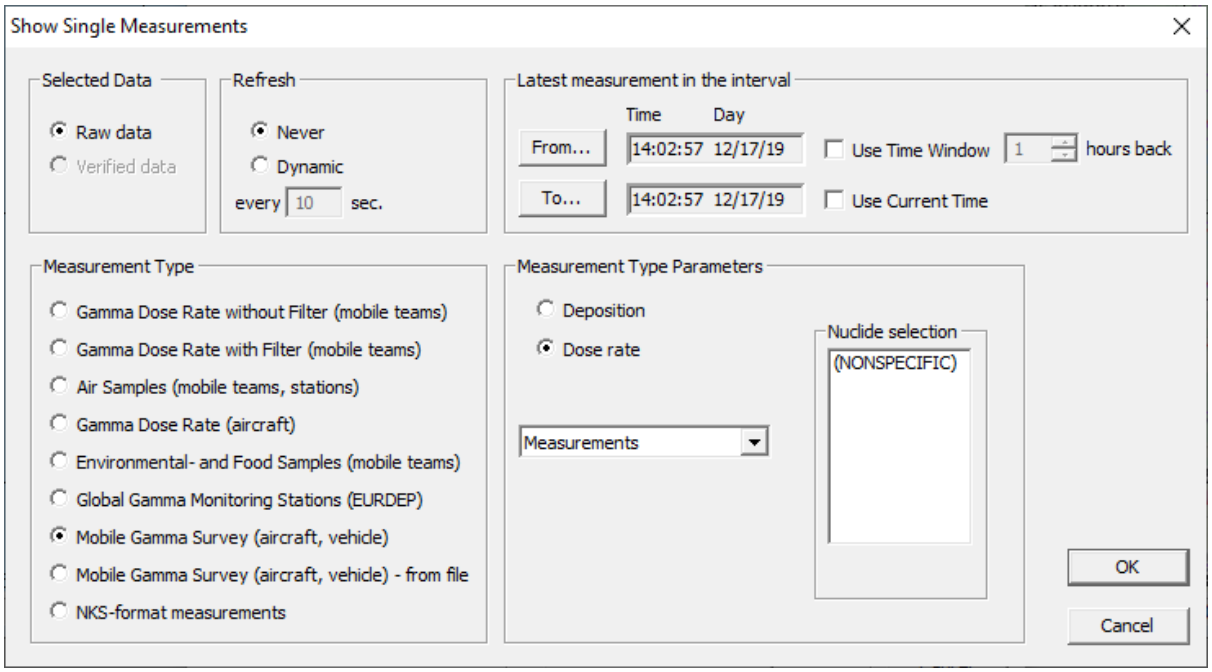

Figure 39 GUI for selecting measurement data to be visualized in the system.

Request interface SL and SC modelling

The request interface should be able to at least provide information from ARGOS to the SL and SC models about

- General
  - List of nuclides
  - List of measurements
  - Position of source if known
- Per measurement
  - Position of measurement
  - Time (time frame) of measurement
  - Air concentration (Bq/m^3) per nuclide
  - Detection limits (per nuclide)
  - Gamma dose rates

In case of too few measurements, ARGOS should be able to receive the reply back from the national meteorological service that the problem is undetermined, and to communicate this to the ARGOS user.

Result interfaces for SL and SC

The result of SL will resemble ordinary dispersion modelling; however, here the results shown on a map will be probability densities for the location of the source. For SC, the model result will to a high degree resemble a source term description, thus it would be quite efficient to reuse the interface for source term description from ARGOS to the ADM models as the interface from SC to ARGOS.

Types of measurements

As can be seen from the GUI for visualising measurements in ARGOS above, ARGOS can handle quite many types of measurements. In order to simplify the GUI, we will restrict the selection for SLC to be limited to:

- Permanent Monitoring Stations – dose rates,
- Air Sampler Stations – air concentrations,

or a combination of the two.

It has to be considered how to distinguish between "lack of data" from a station and "below detection limit measurements". Of course, in the radiological domain there will always be some background radiation.

Permanent gamma-monitors and filter stations

In Europe, many radiological filter station measurements are taken once a week. However, in special cases it is possible to change to daily measurements. From a meteorological perspective, a week can be a long time covering a number of different meteorological phenomena taking place over the station site within the period. Additionally, a week could be longer than the accidental release. Thus, if the intended use of the measurements among other things is to assist in locating the release point or to characterize the source, daily measurements are of much greater value. The filters are changed manually, and in most cases sent by regular mail for analysis. This implies a delay in retrieving the measurement data, and it means that short-lived radionuclei have decayed when the filter is measured.

The detection limit depends first of all on the amount of air drawn through the filter. Thus, the pump efficiency and the measurement period are key parameters for the detection limits, and therefore detection limits vary across Europe. In addition, the presence of many radionuclei on a filter makes it difficult to measure concentrations accurately.

There are currently no international agreements on routine distribution of filter station concentration measurements. For the October 2017 case of Ru-106 measurements in Europe, the IAEA collected the available filter station data (IAEA, 2017a,b).

The European Radiological Data Exchange Platform (EURDEP), see https://eurdep.jrc.ec.europa.eu/Entry/, is a network for the exchange of radiological monitoring data between most European countries. Currently, EURDEP is used for the European automatic gamma monitoring network which does not provide activity concentrations, only gamma dose rates. However, EURDEP might be used also for filter station measurements which could be very helpful in future events.

In comparison with filter-stations, the gamma monitoring network in Europe is much denser and reports automatically at high frequency, e.g. hourly, all of which make such data attractive for an operational nuclear DSS. However, in order to use the gamma-monitoring data for inverse modelling it is beneficial that measurements of nuclide-specific average activity concentrations are provided. Further, the measurement sensitivity is several orders of magnitude worse than for filter stations. Thus, gamma monitoring results are most likely only useful for source localization at the early phase of a nuclear accident. They might, however, be of value for the characterization of the release.

The Comprehensive Nuclear-Test-Ban Treaty Organization (CTBTO) includes a monitoring network of 80 radiological stations measuring radioactive particles, around half of them also noble gasses. Near real time access to these data will be very helpful for locating or characterizing an unknown release of radionuclei.

All in all there is a need for automated and uniform handling of filter station measurements and for a network or an organization to take care of the collection of data and providing them in an organized way for Emergency Management Organizations and DSS systems.

Summary, Conclusions and Outlook

For a source, with a known geographic location, of radionuclides which have been accidentally released to the atmosphere, it is important to estimate the release rates for the dose-contributing nuclides. In the first year of SOCHAOTIC, various methods have been developed for estimation of the release employing measurements of activity concentrations at filter stations as well as gamma dose measurements at gamma monitors. The methods have been applied to three cases, viz. the European Tracer Experiment (ETEX), the 2017 case of Ru-106 in Europe, and an artificial case of a release from the Loviisa nuclear power plant in Finland.

For the selected cases, deterministic numerical weather prediction model data have been obtained from the global model of the European Centre for Medium-Range Weather Forecasts (ECMWF) and from the Harmonie high-resolution non-hydrostatic model. By employing the atmospheric dispersion models DERMA, MATCH, SILAM, and SNAP, four different approaches have been applied in order to estimate the release rates for the selected cases. However, qualitatively these methods have provided quite similar results, and it is therefore not possible to prioritize the methods.

The previous NKS projects MUD (Sørensen *et al.*, 2014), FAUNA (Sørensen *et al.*, 2016) and AVESOME (Sørensen *et al.*, 2019) have demonstrated that inherent meteorological uncertainties play an important role for the atmospheric dispersion model results; see also (Sørensen *et al.*, 2020). In the proposed continuation of the SOCHAOTIC project, we wish to examine the uncertainties of the source estimation arising from the inherent meteorological uncertainties. This will be carried out by applying the methodologies developed in the first year of SOCHAOTIC to an ensemble of numerical weather prediction model results. Subsequently, ensemble-statistical methods will be applied to quantify the uncertainties of the estimated release profiles.

References

Andersson, C., Bergström, R., Bennet, C., Robertson, L., Thomas, M., Korhonen, H., Lehtinen, K.E.J., and Kokkola, H. 2015. MATCH-SALSA – Multi-scale Atmospheric Transport and CHemistry model coupled to the SALSA aerosol microphysics model – Part 1: Model description and evaluation. *Geosci. Model Dev.* **8**, 171–189. doi:10.5194/gmd-8-171-2015

Baklanov, A. and J. H. Sørensen. Parameterisation of radionuclide deposition in atmospheric dispersion models. *Phys. Chem. Earth* **26** (2001) 787–799

Baklanov, A., A. Mahura and J. H. Sørensen. Methodology for Prediction and Estimation of Consequences of Possible Atmospheric Releases of Hazardous Matter: 'Kursk' Submarine Study. Atmos. *Phys. Chem.* Vol. **3** (2003) 747–762

Bartnicki, J., H. Haakenstad, and Ø. Hov. Operational SNAP model for remote applications from NRPA. *Norwegian Meteorological Institute Report* (2011) 12–2011

Bartnicki, J., I. Amundsen, J. Brown, A. Hosseini, Ø. Hov, H. Haakenstad, H. Klein. Atmospheric transport of radioactive debris to Norway in case of a hypothetical accident related to the recovery of the Russian submarine K-27. *Journal of environmental radioactivity* **151** (2016) 404–416

Bengtsson, L., U. Andrae, T. Aspelien, Y. Batrak, J. Calvo, W, de Rooy, E. Gleeson, B. H. Sass, M. Homleid, M. Hortal, K.-I. Ivarsson, G. Lenderink, S. Niemelä, K. P. Nielsen, J. Onvlee, L. Rontu, P. Samuelsson, D. S. Muñoz, A. Subias, S. Tijm, V. Toll, X. Yang, and M. Ø. Køltzow. The HARMONIE–AROME Model Configuration in the ALADIN–HIRLAM NWP System. *Monthly Weather Review* (2017) **145** No. 5 https://doi.org/10.1175/MWR-D-16-0417.1

Casella, G., and George, E. I. (1992). Explaining the Gibbs sampler. *The American Statistician*, *46*(3), 167-174

Eckerman, K.F. and J.C. Ryman. External exposure to radionuclides in air, water, and soil, Federal Guidance Report 12 (1993)

Eckerman, K.F. and R.W. Leggett. DCFPAK 3.02 (Dose Coefficient Data File Package), Oak Ridge National Laboratory (2013)

ETEX web-site (2019), https://rem.jrc.ec.europa.eu/etex/

Gloster, J., A. Jones, A. Redington, L. Burgin, J. H. Sørensen, R. Turner. International approach to atmospheric disease dispersion modelling. *Veterinary Record* 03 (2010a) **166** (12):369. DOI:10.1136/vr.166.12.369a

Gloster, J., A. Jones, A. Redington, L. Burgin, J. H. Sørensen, R. Turner, P. Hullinger, M. Dillon, P. Astrup, G. Garner, R. D'Amours, R. Sellers and D. Paton. Airborne spread of foot-and-mouth disease – model intercomparison. *Veterinary Journal* **183** (2010b) 278–286

Graziani, G., Klug, W., and Nodop, K. Real-time Long-range Dispersion Model Evaluation of the ETEX First Release. **EUR 17754 EN** (1998) 92-828-3657-6 European Commission

Hastings, W. (1970). Monte Carlo sampling methods using Markov chains and their applications. *Biometrika* 57 (1), 97–109

Heinonen, S. (2017) CALCULATION OF GAMMA-RAY DOSE RATE FROM AIRBORNE AND DEPOSITED ACTIVITY. X-ray and gamma-ray decay data standards for detector calibration and other applications. https://www-nds.iaea.org/xgamma_standards/

Hoe, S., J. H. Sørensen and S. Thykier-Nielsen. The Nuclear Decision Support System ARGOS NT and Early Warning Systems in Some Countries around the Baltic Sea. In: Proceedings of the 7th Topical Meeting on Emergency Preparedness and Response, September 14–17, 1999, Santa Fe, New Mexico, USA

Hoe, S., H. Müller, F. Gering, S. Thykier-Nielsen and J. H. Sørensen. ARGOS 2001 a Decision Support System for Nuclear Emergencies. In: Proceedings of the Radiation Protection and Shielding Division Topical Meeting, April 14–17, 2002, Santa Fe, New Mexico, USA

Hoffman, M. D., & Gelman, A. (2014). The No-U-Turn sampler: adaptively setting path lengths in Hamiltonian Monte Carlo. *J. Mach. Learn. Res.*, 15(1), 1593-1623

IAEA. Convention on Early Notification of a Nuclear Accident. (1986) https://www.iaea.org/publications/documents/treaties/convention-early-notification-nuclear-accident

IAEA. Updated Technical Attachment Status of Measurements of Ru-106 in Europe, 2017-10-20, 12:00 UTC, prepared by the Incident and Emergency Centre of the IAEA. Available through national radiation protection authorities. (2017a)

IAEA, Status of Measurements of Ru-106 and Ru-103 in Europe at 2017-11-24, 15:00 UTC, prepared by the Incident and Emergency Centre of the IAEA. Available through national radiation protection authorities. (2017b)

Johansson, Jan, Peder Kock, Jonas Boson, Simon Karlsson, Patrick Isaksson, Jonas Lindgren, Elisabeth Tengborn, Anna Maria Blixt Buhr, Ulf Bäverstam. Review of Swedish emergency planning zones and distances. SSM report (2017) https://www.stralsakerhetsmyndigheten.se/en/publications/reports/radiation-protection/2017/201727e/

Kahnert, M., Variational data analysis of aerosol species in a regional CTM: Background error covariance constraint and aerosol optical observations operators, *Tellus*, 60B, 753-770, (2008)

Kahnert, M. (2018). Information constraints in variational data assimilation. *Q. J. R. Meteorol. Soc.* 144, 2230-2244

Klein, H., and Bartnicki**,** J. (2018). The Severe Nuclear Accident Programme, Concert Air2 Bulletin, Issue 24, 2018, page 4

Lauritzen, B., A. Baklanov, A. Mahura, T. Mikkelsen and J. H. Sørensen. K-model description of probabilistic long-range atmospheric transport in the Northern Hemisphere. *Atmos. Environ.* **40** (2006) 4352–4369

Lauritzen, B., A. Baklanov, A. Mahura, T. Mikkelsen and J. H. Sørensen. Probabilistic risk assessment for long-range atmospheric transport of radionuclides. *J. Envir. Radioactivity* **96** (2007) 110–115

Le Brazidec, J. D., Bocquet, M., Saunier, O., & Roustan, Y. (2020). MCMC methods applied to the reconstruction of the autumn 2017 Ruthenium-106 atmospheric contamination source. *Atmospheric Environment: X*, *6*, 100071

Liu, Y., Haussaire, J. M., Bocquet, M., Roustan, Y., Saunier, O., & Mathieu, A. (2017). Uncertainty quantification of pollutant source retrieval: comparison of Bayesian methods with application to the Chernobyl and Fukushima Daiichi accidental releases of radionuclides. *Quarterly Journal of the Royal Meteorological Society*, 143(708), 2886-2901

Mahura, A., A. Baklanov and J. H. Sørensen. Methodology for evaluation of possible consequences of accidental atmospheric releases of hazardous matter. *Radiat. Prot. Dos.* **103** (2003) 131–139

Mahura, A. G., A. A. Baklanov, J. H. Sørensen, F. L. Parker, V. Novikov, K. Brown, K. L. Compton 2004: Assessment of Atmospheric Transport and Deposition Patterns Related to Russian Pacific Fleet Operations. *Environmental Monitoring and Assessment* **101** (2005) 261–287

Masson, O., Steinhauser, G., Zok, D., Saunier, O., Angelov, H., Babić, D., & Zorko, B. (2019). Airborne concentrations and chemical considerations of radioactive ruthenium from an undeclared major nuclear release in 2017. *Proceedings of the National Academy of Sciences*, *116*(34), 16750-16759

Mikkelsen, T., S. Alexandersen, H. Champion, P. Astrup, A. I. Donaldson, F. N. Dunkerley, J. Gloster, J. H. Sørensen and S. Thykier-Nielsen. Investigation of Airborne Foot-and-Mouth Disease Virus Transmission during Low-Wind Conditions in the Early Phase of the UK 2001 Epidemic. *Atmos. Chem. Phys. Disc.* **3** (2003) 677–703

PDC-ARGOS. http://www.pdc-argos.com

Robertson, L. and Langner, J. 1998. Source function estimate by means of variational data assimilation applied to the ETEX-1 tracer experiment. *Atmos. Environ.* **32**, 4219-4225

Robertson, L., Langner, J. and Engardt, M., An Eulerian limited-area atmospheric transport model, *J. Appl. Met.* 38, 190-210, 1999

Saltbones, J., A. Foss, and J. Bartnicki. Norwegian Meteorological Institute's real-time dispersion model SNAP (Severe Nuclear Accident Program): Runs for ETEX and ATMES II experiments with different meteorological input. *Atmospheric Environment* **32** no. 24 (1998) 4277–4283

Salvatier J., Wiecki T.V., Fonnesbeck C. (2016). Probabilistic programming in Python using PyMC3. *PeerJ Computer Science* 2:e55 DOI: 10.7717/peerj-cs.55

Sofiev, M., Vira, J., Kouznetsov, R., Prank, M., Soares, J., and Genikhovich, E. Construction of the SILAM Eulerian atmospheric dispersion model based on the advection algorithm of Michael Galperin. *Geosci. Model Devel*. (2015) **8** 3497–3522

Sørensen, J.H., Bartnicki, J., Blixt Buhr, A.M., Feddersen, H., Hoe, S.C., Israelson, C., Klein, H., Lauritzen, B., Lindgren, J., Schönfeldt, F., Sigg, R. Uncertainties in atmospheric dispersion modelling during nuclear accidents. *J. Environ. Radioact.* **222** (2020) 1-10 https://doi.org/10.1016/j.jenvrad.2020.106356

Sørensen, J. H. Sensitivity of the DERMA Long-Range Dispersion Model to Meteorological Input and Diffusion Parameters. *Atmos. Environ.* **32** (1998) 4195–4206

Sørensen, J. H., D. K. J. Mackay, C. Ø. Jensen and A. I. Donaldson. An integrated model to predict the atmospheric spread of foot-and-mouth disease virus. *Epidemiol. Infect.* (2000) 124, 577–590

Sørensen, J. H., C. Ø. Jensen, T. Mikkelsen, D. Mackay and A. I. Donaldson. Modelling the atmospheric spread of foot-and-mouth disease virus for emergency preparedness. *Phys. Chem. Earth* **26** (2001) 93–97

Sørensen, J. H., A. Baklanov and S. Hoe. The Danish Emergency Response Model of the Atmosphere. *J. Envir. Radioactivity* **96** (2007) 122–129

Sørensen, J. H., B. Amstrup, H. Feddersen, U. S. Korsholm, J. Bartnicki, H. Klein, P. Wind, B. Lauritzen, S. C. Hoe, C. Israelson, and J. Lindgren. Meteorological Uncertainty of atmospheric Dispersion model results (MUD). **NKS-307** ISBN 978-87-7893-385-0, http://www.nks.org/en/nks_reports/view_document.htm?id=111010212220490 (2014)

Sørensen, J.H., B. Amstrup, H. Feddersen, J. Bartnicki, H. Klein, M. Simonsen, B. Lauritzen, S. C. Hoe, C, Israelson and J. Lindgren. Fukushima Accident: UNcertainty of Atmospheric dispersion modelling (FAUNA). **NKS-360** ISBN 978-87-7893-444-4 (2016), http://www.nks.org/scripts/getdocument.php?file=111010213440189

Sørensen, J. H., Schönfeldt, F., Sigg, R., Pehrsson, J., Lauritzen, B., Bartnicki, J., Klein, H., Hoe, S. C., and Lindgren, J. Added Value of uncertainty Estimates of SOurce term and Meteorology (AVESOME) – final report. NKS-420, ISBN 978-87-7893-509-0 (2019) http://www.nks.org/en/nks_reports/view_document.htm?id=111010214696230

Tølløse, K. S., Kaas, E., & Sørensen, J. H. (2021). Probabilistic Inverse Method for Source Localization Applied to ETEX and the 2017 Case of Ru-106 including Analyses of Sensitivity to Measurement Data. *Atmosphere*, *12*(12), 1567

Acknowledgements

NKS conveys its gratitude to all organizations and persons who by means of financial support or contributions in kind have made the work presented in this report possible.

Disclaimer

Bibliographic Data Sheet **NKS-458**

Title	SOurce CHAracterizatiOn accounting for meTeorologIcal unCertainties (SOCHAOTIC) – first-year report
Author(s)	Jens Havskov Sørensen[1] (co-ordinator) Henrik Feddersen[1] Kasper Skjold Tølløse[1] Rostislav Kouznetsov[2] Mikhail Sofiev[2] Andreas Uppstu[2] Heiko Klein[3] Magnus Ulimoen[3] Lennart Robertson[4] Jan Pehrsson[5] Bent Lauritzen[6] Dan Bohr[7] Agnieszka Hac-Heimburg[7] Carsten Israelson[7] Einar Améen[8] Anna Maria Blixt Buhr[9] Jonas Lindgren[9] Tuomas Peltonen[10]
Affiliation(s)	[1]Danish Meteorological Institute (DMI) [2]Finnish Meteorological Institute (FMI) [3]Norwegian Meteorological Institute (MET Norway) [4]Swedish Meteorological and Hydrological Institute (SMHI) [5]PDC-ARGOS [6]Technical University of Denmark (DTU) [7]Danish Emergency Management Agency (DEMA) [8]Norwegian Radiation and Nuclear Safety Authority (DSA) [9]Swedish Radiation Safety Authority (SSM) [10]Radiation and Nuclear Safety Authority (STUK)
ISBN	978-87-7893-551-9
Date	April 2022
Project	NKS-B / SOCHAOTIC
No. of pages	57
No. of tables	1
No. of illustrations	40
No. of references	48

Abstract
max. 2000 characters

In recent years, events have occurred in which radionuclides were detected by filter stations in European countries without knowledge on the origin of those radionuclides. In such cases, there is a need to locate potential release sites. However, if the release site is actually known, or if a potential release site has been localized by inverse methods, then there is an additional need to estimate the release rates from this location as a function of time for the various radionuclides detected.

While in the SLIM NKS project, methodologies were developed to localize an unknown source of radionuclides dispersed in the atmosphere, the SOCHAOTIC project develops methodologies, suited for operational use, by which characterization of the source, whose location is known, can be derived, i.e. to estimate the temporal release profiles of the radionuclides detected.

For operational use, nuclear decision-support systems should be extended with modules handling and analysing such monitoring data automatically, and conveying the data together with the geographical coordinates of the release point to the national meteorological centre accompanied by a request to estimate the temporal evolution of the release rates.

In the first year of SOCHAOTIC, the following results are obtained:

- Case studies identified and selected, viz. the ETEX-1 and the October 2017 case of Ru-106 in Europe. In addition, an artificial case is produced by running a dispersion model forward and calculating average concentrations at filter stations and gamma dose rates at nearby gamma stations.
- Methods for estimation of the temporal release profiles are developed, implemented and described.
- Deterministic numerical weather prediction model data are derived.
- Quality-controlled measurement data of ground-level concentration are obtained.
- The methods for source term characterization are applied by using the DERMA, MATCH, SILAM and SNAP atmospheric dispersion models.
- Results are intercompared.

Key words

nuclear emergency preparedness, atmospheric dispersion modelling, source characterization, inverse modelling, concentration measurements, gamma dose measurements, uncertainty